International Journal of Heat and Mass Transfer 194 (2022) 123085

Contents lists available at ScienceDirect

International Journal of Heat and Mass Transfer

journal homepage: www.elsevier.com/locate/hmt

Staggered oriented airfoil shaped pin-fin heat sink: Investigating the efficacy of novel water based ferric oxide-silica hybrid nanofluid

Hamza Babar[a], Hongwei Wu[a,*], Hafiz Muhammad Ali[b,c,*], Tayyab Raza Shah[d,e], Wenbin Zhang[f]

[a] School of Physics, Engineering and Computer Science, University of Hertfordshire, Hatfield AL10 9AB, United Kingdom
[b] Mechanical Engineering Department, King Fahd University of Petroleum & Minerals (KFUPM), Dhahran 31261, Saudi Arabia
[c] Interdisciplinary Research Center for Renewable Energy and Power Systems (IRC-REPS), King Fahd University of Petroleum and Minerals, Dhahran 31261, Saudi Arabia
[d] Mechanical Engineering Department, NFC Institute of Engineering and Technology, Multan, Pakistan
[e] College of Engineering, Peking University, Beijing, China
[f] School of Science and Technology, Nottingham Trent University, Clifton Lane, Nottingham NG11 8NS, United Kingdom

ARTICLE INFO

Article history:
Received 24 February 2022
Revised 11 May 2022
Accepted 28 May 2022
Available online 11 June 2022

Keywords:
Heat sink
Hybrid nanofluid
Electronic cooling
Thermal management
Airfoil

ABSTRACT

Nowadays, electronic components are one of the essential parts of almost every smart device. To efficiently transfer the desired amount of heat, recent studies have focused on investigating the potential of advanced thermal coolants and heat sink configurations. Current study reveals the potential of novel water-based hybrid nanofluid of silica (SiO_2) and ferric oxide (Fe_2O_3) for cooling high-heat-generating electronic devices. The experimental work was conducted to inspect the heat transfer characteristics of a uniquely designed staggered oriented airfoil shaped pin-fin heat sink employing Fe_2O_3-SiO_2 hybrid nanofluid with different mixture ratios (25%:75%), (50%:50%), (75%:25%). Airfoil shaped pin-fins offer less resistance to fluid flow and maximum effective area due to their unique shape and delayed separation of fluid at the rear end. All the mixture ratios were tested at three different heating powers (75, 100, 125 W) with varying Reynolds number in laminar flow regime. Experimental results revealed that the fluid having a mixture ratio of 50:50 showed the least thermal resistance followed by 25:75 and 75:25. Maximum enhancement of 17.65% in average Nusselt number was observed against the heating power of 75W. Pumping power was found to increase with the supplementation of nanoparticles in base fluid, while a little variation was observed among different mixture ratios. Finally, the results were compared with recently published studies, which revealed that the airfoil shaped fins have better thermal characteristics and offer less resistance to fluid flow.

1. Introduction

Technological advancements demand compact devices that pose significant challenges to researchers and developers. It is a daunting task to design a sink within the size limits of the system. Conventional fluids such as oils, water, ethylene glycol, acetone, etc., failed to transfer the desired amount of heat due to smaller thermal conductivity values. That is why researchers are moving towards hybrid cooling techniques to transfer excessive heat and maintain the devices within a safe temperature threshold. A fluid with enhanced thermal characteristics is used in combination with miniature heat sinks. Investigators found that supplementation of non-metallic or metallic nano-sized particles in base fluid considerably improved the fluid thermal characteristics [1–3]. For compact systems such as microprocessors to effectively transfer the excessive amount of heat micro channel heat sinks employing nanofluids as a working fluid is the most efficient technique due to fewer requirements of cooling agent and larger surface area to volume ratio [4,5].

The work carried out by Abbassi et al. [6] on rectangular-shaped mini-channels with Cu/water nanofluid suggested that an increase in heat transfer can be achieved by influencing the flow or changing the flow from laminar to the turbulent regime. Wu et al. [7] inspected the convective heat transfer and pressure drop employing the nanofluid of alumina and compared the results with the base fluid (water). The trapezoidal shaped silicon-based mini-channel

* Corresponding authors.
E-mail addresses: h.babar@herts.ac.uk (H. Babar), h.wu6@herts.ac.uk (H. Wu), hafiz.ali@kfupm.edu.sa (H.M. Ali), wenbin.zhang@ntu.ac.uk (W. Zhang).

https://doi.org/10.1016/j.ijheatmasstransfer.2022.123085

Nomenclature

Al_2O_3	*alumina, aluminum oxide*
Ag	*silver*
ASPFHS	*airfoil shaped pin-fin heat sink*
CNTs	*carbon nanotubes*
CNC	*computer numerical control*
CPU	*central processing unit*
CTAB	*cetyltrimethylammonium bromide*
Cu	*copper*
DW	*distilled water*
EG	*ethylene glycol*
Fe_2O_3	*ferric oxide*
H	*height*
HTC	*heat transfer coefficient*
LFR	*laminar flow regime*
LMTD	*logarithmic mean temperature difference*
MAE	*mean absolute error*
MCHS	*mini channel heat sink*
MgO	*magnesium oxide*
MWCNT	*multiwalled carbon nanotubes*
NACA	*National Advisory Committee for Aeronautics*
PEC	*performance evaluation criterion*
PD	*pressure drop*
PP	*pumping power*
SDS	*sodium dodecyl sulfate*
SiO_2	*silica, silicon dioxide*
TiO_2	*titanium dioxide, titania*
ZnO	*zinc oxide*

Symbols

A	*surface area* $[m^2]$
AR	*aspect ratio*
$A_{ss,\ top}$	*top surface area of fin* $[m^2]$
$A_{ss,\ side}$	*side surface area of fin* $[m^2]$
C_p	*heat capacity* $[J/kg\ ^\circ C]$
D	*diameter [m]*
d_h	*hydraulic diameter [m]*
f	*friction factor*
h	*heat transfer coefficient* $[W/m^2\ ^\circ C]$
k	*thermal conductivity* $[W/m\ ^\circ C]$
L	*length [m]*
L_{fin}	*length of fin [m]*
M	*molecular weight*
m	*mass [kg]*
$\dot{m}$	*mass flow rate* $[kg/s]$
N	*Avogadro's number*
n	*empirical shape factor*
ΔP	*pressure drop [bar]*
Pr	*Prandtl number*
P_{fin}	*perimeter of fin [m]*
Q	*heat transfer rate [W]*
R_{th}	*thermal Resistance* $[m^2\ ^\circ C/W]$
Re	*Reynolds number*
T	*temperature* $[^\circ C]$
$U_{exp.}$	*experimental quantity*
$U_{pred.}$	*predicted quantity*
V	*volumetric flow rate*
v	*fluid velocity*
V_{fin}	*volume of fin*
W	*width [m]*

Greek letter

φ	*particle concentration [%]*
ρ	*density* $[kg/m3]$
μ	*viscosity* $[kg/m.s]$

Subscript

b	*base*
bf	*base fluid*
C	*coolant*
eff	*effective*
hnf	*hybrid nanofluid*
f	*fin*
nf	*nanofluid*
np	*nanoparticle*
p	*particle*
s	*Heat sink*
ss	*specific section*
sef	*sink effective area*
w	*wall*

heat sink (MCHS) was analyzed considering the effect of particle volume fraction, Prandtl number, and Reynolds number. It was found that the friction factor and pressure drop were increased marginally compared to the conventional fluid. However, the Nusselt number (Nu) was also improved with Reynolds number, particle concentration, and Prandtl number. They also noticed the nanoparticles deposition on the walls, which becomes more significant at higher temperatures. Mohammed et al. [8] numerically examined the important factors such as heat transfer coefficient (HTC), wall temperature, pressure drop, thermal resistance, friction factor, and wall shear rate in rectangular-shaped mini channel heat sinks employing alumina (Al_2O_3)/water nanofluid. They observed that the HTC augmented up to a certain particle concentration limit. It was revealed that the results became identical to the water at 5 vol.%. Factors such as wall shear rate and friction factor increased slightly with particle addition, while thermal resistance reduced. On the other hand, the pressure drop increased as the Reynolds number and particle loading increased. Alazwari and Safaei [9] investigated the effect of copper nanofluid varying concentration in the range of 0.0–4.0% at very low Reynolds number (10–80). The results showed an improvement of 42.3% in heat transfer with a slight increase in pressure drop.

Moghadassi et al. [10] studied the thermal performance of unitary and hybrid nanofluids of Al_2O_3 and Al_2O_3-Cu in a uniformly heated circular tube and found that the binary fluid presents the better results, however, this usually depends on the combination of nanoparticles. It was concluded that the hybrid nanofluid showed an augmented Nusselt number of 4.73% relative to the unitary nanofluid of alumina. The study conducted by Al-Shamani et al. [11] employed the nanofluids of SiO_2, ZnO, Al_2O_3, and CuO through rib grooved heat sink altering the factors such as Reynolds number, particle diameter, volume fraction ranging from $(40,000 \geq Re \leq 10,000)$, $(70nm \geq d_p \leq 25nm)$, $(4 \geq \varphi \leq 1)$ respectively. According to the results, the Nu was found to increase with an increase in particle volume fraction and flow rate while a decreasing trend was observed with an increase in particle diameter. It was also revealed that SiO_2 nanofluids delivered the highest value of Nu in comparison of other examined fluids. Nimmagadda and Venkatasubbaiah [12] compiled a comparative study on the heat transfer enhancement of the nanofluids of alumina, silver (Ag) and their hybrid (Ag+ Al_2O_3) in a rectangular shaped MCHS. It was observed that hybrid nanofluid with a volume fraction of 3% (Ag (2.4%) + Al_2O_3(0.6%)) delivered a higher rate of heat transfer compared to the metallic (Ag) and oxide (Al_2O_3) nanofluids. They recommended the hybrid nanofluids because it was found to be more stabilized and cost-effective. Duangthongsuk and Wongwises [13] studied the hydraulic and thermal performance of a circular

finned heat sink using water-based SiO_2 and ZnO nanofluids. The comparative study showed an improvement of 3 to 9% for the ZnO nanofluid compared to SiO_2. Moreover, pressure drop was found to be increased with flow rate and particle concentration.

Abdollahi et al. [14] used a heat sink with a V-type inlet/outlet to examine the thermal and hydrodynamic performance of various nanofluids (ZnO, SiO_2, Al_2O_3, and CuO). This numerical study also considered the effect of particle concentration and particle diameter. It was observed that the thermal performance of SiO_2 nanofluid was maximum followed by CuO, Al_2O_3, and ZnO, while CuO nanofluid offered less pressure drop followed by Al_2O_3, ZnO, and SiO_2. Results revealed that the effect of particle volume fraction was more significant, however, a noticeable enhancement in Nu was also observed with decreasing particle diameter. Zhou and Catton [15] studied numerically the hydrothermal performance of different plate fin heat sinks having different pin fin shapes (dropform, circular, square, NACA profile, and elliptical). Recirculation zones at the rear end of pin fins were observed. Flow separated at the rear end because of stationary recirculation and reattached again, resulting in the formation of a dead zone. Velocity streamlines illustrated that flow separation was most prominent for square pin fins due to sharp edges. Interestingly, the Nusselt number for square pin fins was comparatively higher, but at the same time, pressure drop was also much higher. So, the comparison was drawn based on the heat transfer effectiveness factor and found that elliptical and NACA shaped pin fins with plate fins delivered the best results. Table 1 summarized the important parameters of some additional research conducted on different geometrical configurations of heat sinks employing various nanofluids.

In the past few decades, nanofluids have attracted the attention of scholars and investigators due to their improved thermal characteristics. Hybrid cooling (nanofluids in a combination of minichannel heat sink) has proven to be an effective technique for the thermal management of high heat-generating devices. The idea behind the selection of hybrid nanofluids is their better stability period and cost-effectiveness. The unitary silica nanofluid showed better stability but not good thermally due to its poor thermal conductivity. On the other side, ferric oxide nanofluid has better thermal characteristics but comparatively lower stability period, because the ferric oxide has higher density value. As the results demonstrate that the sample with an equal mixture ratio (50:50) performed better than the fluid with higher concentration of ferric oxide. In addition, ferric oxide nanoparticles are also cost-effective. However, the addition of nanoparticles in base fluid also increases the pumping power. In fact, the performance of heat sink cannot be decided on the basis of heat transfer only. It is the trade-off of pumping power and heat transfer. Thus, pumping power is also a predominant factor that can be reduced by selecting an appropriate design of heat sink. So, both aspects should be considered while designing a heat sink. Airfoil shape has proven to be effective because it provides less resistance to fluid flow while offering substantial effective surface area for heat transfer. According to Ho et al. [16], fins orientation caused the formation of vortices results to enhance the rate of heat transfer. Results also yielded that fins having angle above 10° restricted the fluid flow and increased the pumping power. A small improvement in heat transfer with a significant increase in pumping power is undesirable. That is why, the fins have been oriented at an angle of 5° clockwise and anticlockwise. It will increase the flow resistance slightly but improve heat transfer significantly. Heat transfer can be improved by increasing the fins orientation, but it costs in the form of pumping power [17].

Fig. 1 depicts the stats of the "Web of Science" searched with a keyword of "airfoil" and "nanofluid". The results were then filtered with different keywords to highlight the novelty of this study. No doubt, numerous studies have been compiled on airfoil profiles in different applications [18–27], as shown in Fig. 1(a). Most of the studies carried out on airfoil profile in the fields of mechanical and aerospace. However, the literature reports very limited studies on airfoil shaped pin-fin heat sinks (ASPFHS). The reported studies numerically examined the performance of heat sinks using air, supercritical carbon dioxide, etc. as a cooling agent [16,28–30]. However, till 2020, not even a single experimental study has been reported in the literature that examined the hydrothermal performance of staggered oriented ASPFHS using water or nanofluid as a cooling agent. In addition, the studied hybrid nanofluid of (Fe_2O_3-SiO_2/water) has also not been investigated before, as illustrated in Fig. 1(b). The presented study aims to emphasize the significance of ASPFHS and hybrid nanofluid mixing ratios to augment the rate of heat transfer.

2. Nanofluid preparation

The current study used the most commonly employed two-step method to prepare the samples of hybrid nanofluids. A number of research articles compiled by different investigators have stated that the two-step method among several is the most effective one for nanofluid preparation. This technique involves two steps; first step deals with the nanoparticles synthesis while these synthesized nanoparticles are dispersed in base fluid in the second step. To ensure the proper mixing and avoid the agglomeration of the particles in base fluid the solution is further treated with the help of magnetic stirrer, ultrasonicator, and homogenizer. Some kinds of surfactants have also been used to enhance the stability period [37]. Shoghl et al. [38] performed the magnetic stirring for 1 h and ultrasonic vibration for 4 h to prepare the stabilized nanofluid of MgO. The study of Ali et al. [39] on the thermal performance of car radiator using MgO nanofluid employed a two-step method for nanofluid preparation. It was observed that the stability of the fluid increased by making it more acidic or decreasing the pH value. For this purpose, they used HCL and noted that after adding HCL to the MgO solution, it turned transparent, and no sedimentation was found even after 7 days. Mahbubul et al. [40] studied the effect of ultrasonication time on the stability of titania nanofluid. Positive impact of ultrasonication was observed on the suspension of particles in base fluid. In addition, it was revealed that reagglomeration of particles begins after performing the sonication process for more than 150 min.

Ghadimi and Metselaar [41] observed that surfactant supplementation while performing the ultrasonication process exhibited improved thermal properties. Zouli et al. [42] followed the two-step method for preparing the Fe_2O_3-water nanofluid. The samples were homogenized for 45 minutes using an IKA homogenizer (T25) and sonicated for 30 minutes to ensure the proper mixing. Four different samples with the particle concentration of (0.01 vol.%, 0.02 vol.%, 0.05 vol.%, and 0.09 vol.%) were prepared and investigated the variation of thermal conductivity with particle concentration and temperature. It was observed that the thermal conductivity increased with temperature and volume fraction of the particles. Kumar and Sonawane [43] also observed an enhancement in thermal conductivity with increasing temperature and particle concentration. Ferric oxide nanoparticles were dispersed in water and ethylene glycol base fluids to prepare the samples with different particle concentrations (0.01-0.08 vol.%). Then, the ultrasonication process was performed for 50 minutes to homogenize the solution. Phuoc and Massoudi [44] prepared the samples of Fe_2O_3-water having a particle diameter of 20 to 40 nm and concentration in the range of (0.01-0.04% by volume) to observe the variation in viscosity. To disperse the particles in water, magnetic stirring and ultrasonication was carried out for half an hour. Parsian and Akbari [45] adopted the two-step method to prepare the ethylene-glycol based hybrid nanofluids of copper and alumina. The samples were

Table 1
Summary of the various experimental and numerical studies conducted on heat sinks for electronic cooling using nanofluids.

Reference	*Study Type*	*Sink Type*	*Heat Sink Material*	*Channel Hydraulic Diameter*	*Reynolds Number*	*Nanofluid*	*Particle Concentration*	*Nusselt Number*	*Pressure drop*	*Other important Factors*
[7]	Experimental	Rectangular	Silicon	194.5 μm	190–1020	Al_2O_3/water	0.15, 0.26 vol.%	Increased 10.2–15.8% by 0.26 vol%.	Increased 3.4–5.5% by 0.26 vol%.	Thermal resistance reduced 11.5% by 0.26 vol.%. Particles deposited on the walls at higher temperature.
[8]	Numerical	Rectangular	–	339.15 μm	100–1000	Al_2O_3/water	1–5 vol.%	–	–	Thermal resistance reduced and pumping power increased 57.6% and 0.0173 W by 5 vol.% respectively.
[11]	Numerical	Rib grooved	–	–	10,000–40,000	SiO_2/water, ZnO/water, Al_2O_3/water, and CuO/water	1–4 vol.%	–	–	–
[12]	Numerical	Rectangular	–	–	200–600	Al_2O_3/water, Ag/water, Ag-Al_2O_3/water	3 vol.%	–	–	HTC enhanced by 26–148%, 111–144%, and 17–18% for Ag+Al_2O_3, Ag, and Al_2O_3 respectively.
[13]	Experimental	Circular pin fin	Aluminum	1.2 mm	700–3800	SiO_2/water, ZnO/water	0.2–0.6 vol.%	–	Increased with particle concentration and flow rate while observed no effect of particle type.	3-9% increase for ZnO compared to SiO_2 in the concentration range of (0.2-0.6 vol.%)
[14]	Numerical	Micro channel with V-type inlet/outlet	Silicon	–	–	SiO_2/water, Al_2O_3/water, ZnO/water, CuO/water	1.0, 1.5, 2.0 vol.%	Increased with an increase in particle concentration and decrease of particle diameter	Increased with particle concentration and particle diameter	–
[31]	Experimental	Rectangular	Copper	8 mm	2985–9360	CuO/water	0.1, 0.2 vol.%	–	–	Pumping power increased by 15.11 % by 0.2 vol.%
[32]	Experimental	Rectangular	Copper	–	133–1515	Al_2O_3/water	0.5–10 wt.%	–	–	HTC increased 72% by 10 wt.
[33]	Numerical	Trapezoidal grooved	–	–	266–799	Al_2O_3/water, CuO/water, ZnO/water, SiO_2/water	1–4 vol.%	Increased 120.22% in trapezoidal grooved MCHS compared to simple MCHS	–	Friction factor increased up to 52.24%.
[34]	Experimental	Rectangular	Aluminium	–	100–5000	CuO/water	0.24, 1.03, 4.5 vol.%	–	Increased 70% by 4.5 vol.%	–
[35]	Experimental	Rectangular	Copper	–	395–989	Al_2O_3/water	0.1–0.25 vol.%	–	–	HTC increased 18% and thermal resistance reduced 15.72% by 0.25 vol.% and
[36]	Experimental	Rectangular	Copper	–	–	Al_2O_3/water	0.05–0.2 vol.%	–	–	Frictional effects found to increase with the supplementation of nanoparticles in the base fluid.

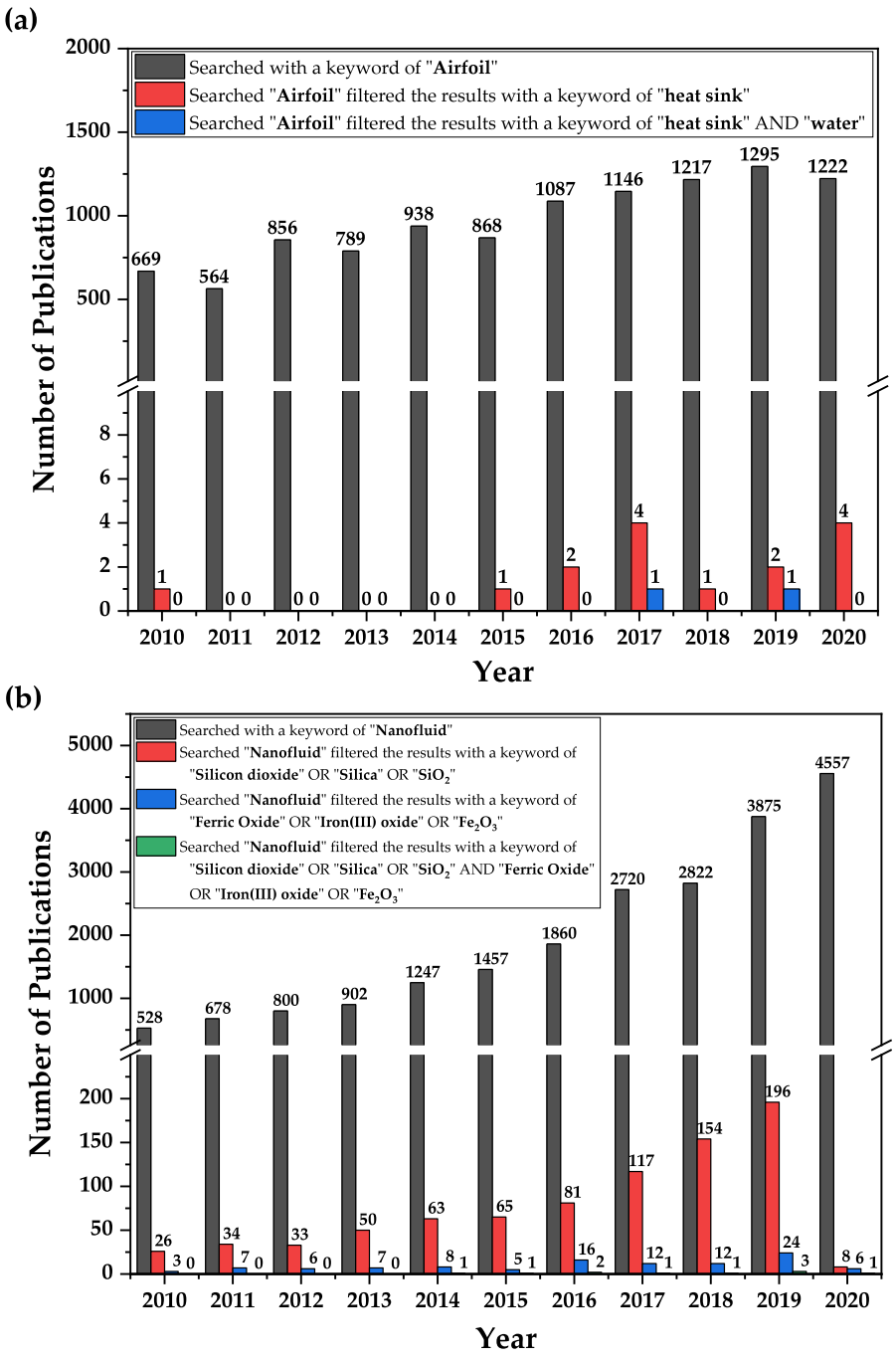

Fig. 1. Web of Science year-wise stats of the number of published articles (2010-2020).

prepared with various concentrations ranging (0.125-2.0 vol.%) considering a particle mixing ratio of 50:50. To break the clusters and make suspension more homogeneous the sonication process was carried out for 7h. The solution prepared adopting this method was found to be stabilized for 3 days. For the preparation of MWCNT-Al_2O_3 (15:85)/oil hybrid nanofluid, Asadi et al. [46] used two-step approach. To obtain a stable solution, magnetic stirring was performed for 2 hours prior to 1 hour of sonication.

To get the hybrid nanofluids of Fe_2O_3-SiO_2/water having different mixture ratios (25:75, 50:50, 75:25), ferric oxide and silica nanofluids were prepared separately with a particle concentration of 0.015 vol.% and mixed accordingly while carrying out continuous stirring with the help of a magnetic stirrer. To ensure the proper mixing of fluids, the processed solution was homogenized for 5 min at 8000rpm. Table 2 details the particle properties and morphology purchased from the market (NanoAmor, USA).

The unitary nanofluid of ferric oxide and silica was prepared by adopting the following steps: added the calculated amount of nanoparticles in the desired quantity of base fluid while stirring, the solution was stirred, homogenized, and sonicated for 30 min, 5 min, and 3 h respectively with the help of magnetic stirrer, IKA T25 homogenizer, and ultrasonicator (frequency 50 kHz). Fig. 2 provides the schematic illustration of the preparation process step by step. To keep the temperature constant, cold water flows around the particles suspended fluid during sonication. The prepared fluids stability was observed for 12 hours and found to be stabilized. A small amount of CTAB surfactant (0.05 g in the 1000 ml solution) was used to improve the stability. Fig. 3 shows the nano-powders,

Table 2
Particle properties.

Particle	Morphology	Size (nm)	Purity	Thermal conductivity (W/m.K)	Density (kg/m^3)	Specific heat (J/kg.K)	References
Fe_2O_3 (alpha)	Spherical	30-50	99%	20	5250	650	[47]
SiO_2	Spherical	20	99+%	1.4	2220	745	[48]

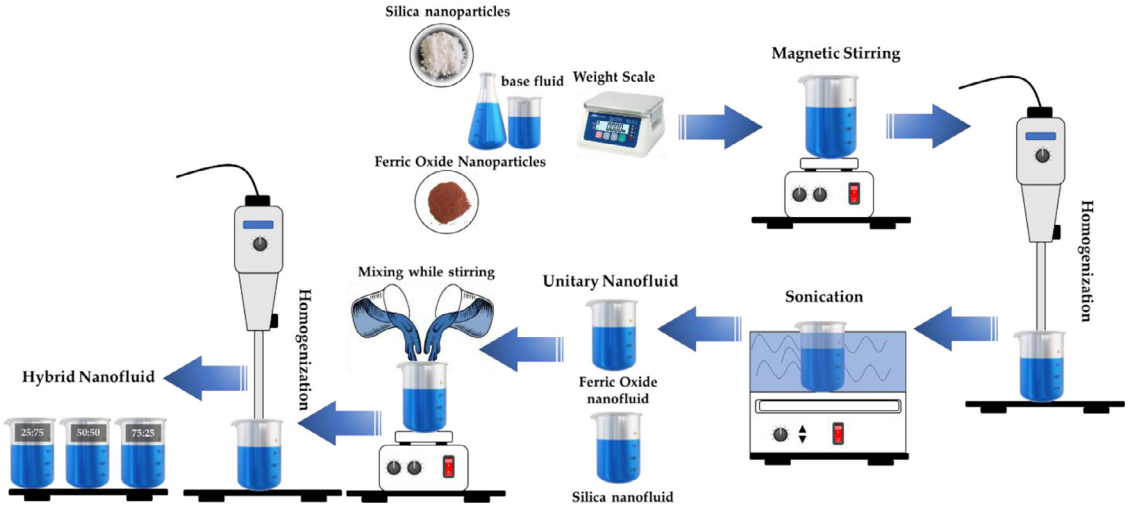

Fig. 2. Schematic illustration of the preparation process.

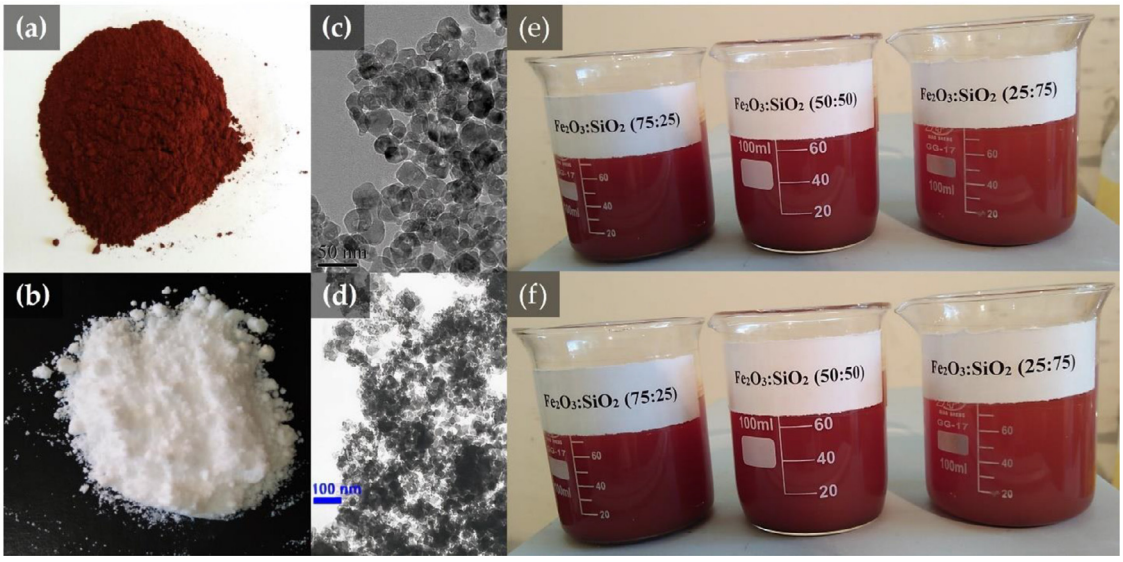

Fig. 3. (a) Ferric oxide nanopowder, (b) silica nanopowder, (c) TEM image of Fe_2O_3 nanparticles (nanoamor), (d) TEM image of SiO_2 nanparticles (nanoamor) (e) nanofluid just after sonication, and (f) nanofluid after 12h.

TEM images, and the prepared samples of hybrid nanofluid of ferric oxide and silica just after the sonication process and after 12 hours.

3. Experimental setup

Experimental setup used to study the heat transfer characteristics and pressure drop of staggered oriented pin-fin heat sink comprised of the interconnection of seven components: a needle valve, pressure transducer, radiator, sink assembly, flow measuring device, pump, and coolant storage tank. Fig. 4 provides the detailed description of experimental setup and coolant flow cycle with the help of a schematic illustration.

Coolant was pumped from the storage tank with the help of a small ac pump (VSS 950, Pakistan). The flow was regulated with the help of a flow control valve connected just after the pump. To measure the rate of circulating fluid, a precise flow measuring device (FTB333D, Omega, USA) was interconnected between the needle valve and heat sink assembly. Three cartridge heaters have been inserted inside the heat sink to provide a constant heat flux. A DC Power Supply (6575A, Agilent, USA) was responsible to supply the desired power to the heaters. Coolant flows through the sink channels continuously carries the heat provided by the heaters. The ends of the pressure transducer purchased from Omega, USA, were connected to the outlet and inlet in a parallel manner using a Y-type connector to precisely measure the pressure drop across the heat sink.

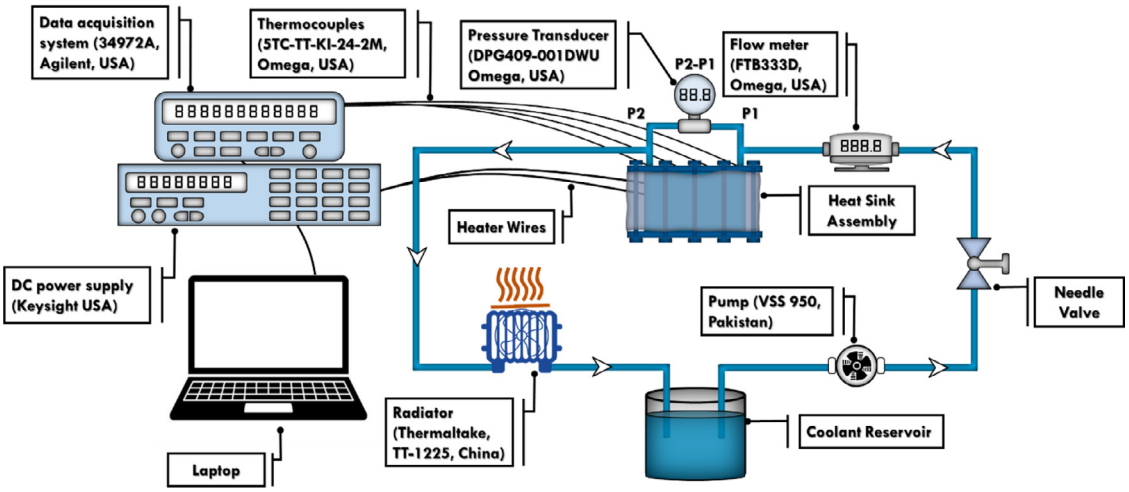

Fig. 4. Schematic illustration of experimental setup and coolant flow cycle.

Table 3
Measuring equipment accuracy.

Equipment	Power Supply	Thermocouple	Pressure Transducer	Flow Meter
Accuracy	Current ± 0.1% Voltage ± 0.04%	± 0.1°C	± 0.08%	± 6%

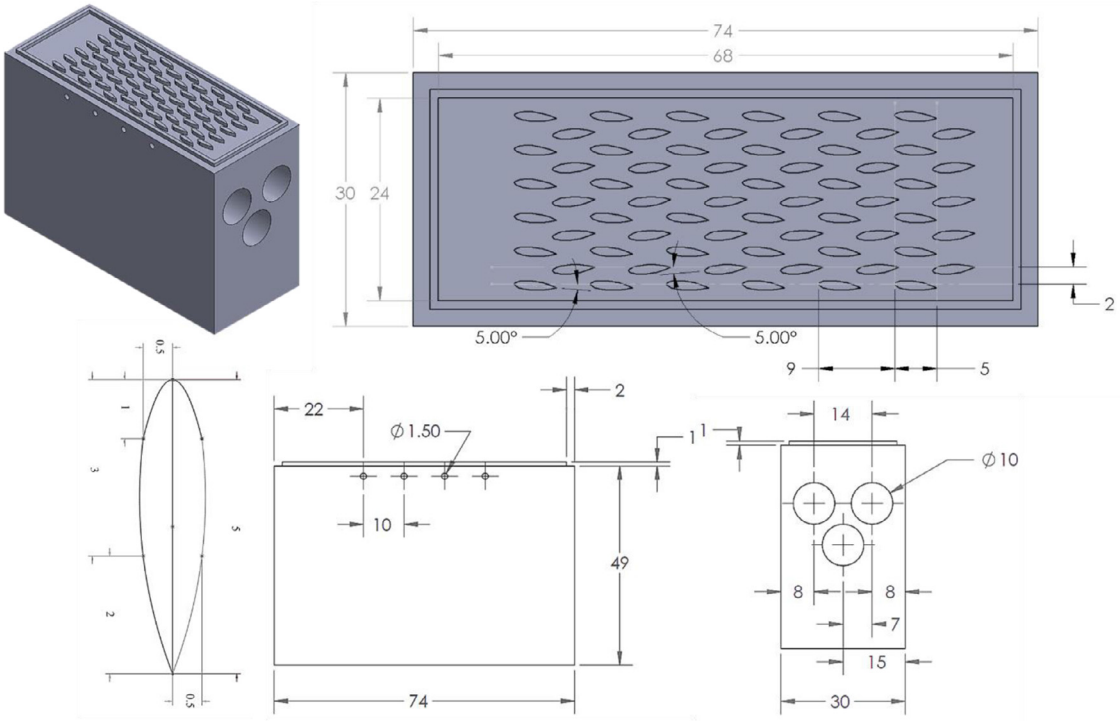

Fig. 5. Geometric configuration of staggered oriented pin-fin heat sink.

Four thermocouples (5TC-TT-KI-24-2M, Omega, USA) were installed at the base 2 mm under the wall of the heat sink channel, one at the inlet and one at the outlet of heat sink to record temperature values. The other ends of the thermocouples were connected with a data logger (Agilent, USA, 34972A) that recorded the temperature after every 5 sec time intervals. Fluid flowing through the channels rejected the heat carried from the sink to the atmosphere by passing through the radiator attached just after the heat sink. Finally, heat carrying fluid transferred into the storage tank to complete the loop. Table 3 shows the accuracy of devices used in the experiment. Fig. 5 shows the isometric and top view of heat sink with a complete description of design and positioning of thermocouples and heaters. The designed heat sink was used for experimental testing with the goal to examine the thermal performance of symmetrical airfoil geometrical configuration. To ensure proper sizing and precision, the sink was manufactured by CNC machining. The fin spacing was designed based on the fact that the 1mm toll bit can be used for production without incurring a severe cost penalty. Furthermore, a reduction in spacing would result in an increase in pumping power. The heat sink's dimensions can be

selected depending on the system's design and requirements. For example, in current study, the heat sink dimensions were 74mm x 42mm which corresponded to the size of the Aries FPGA Module (M100PFS). The fin was 5mm long, with a 1mm head, 2mm tail, and 2mm body. The width at the section partition was 1mm and the spline curve connected the head to tail followed by the body partition.

4. Data processing

To compute the nanoparticles mass (m_{np}) added in water (base fluid) relative to the volume fraction (φ) of particles studied, authors used correlation represented with Eq. (1).

$$\varphi = \left[\frac{\frac{m_{np}}{\rho_{np}}}{\frac{m_{np}}{\rho_{np}} + \frac{m_{bf}}{\rho_{bf}}} \right] \tag{1}$$

$$\frac{k_{hnf}}{k_{bf}} = \frac{\left(\frac{(\varphi_{p1}k_{p1}+\varphi_{p2}k_{p2})}{\varphi} + (n-1)k_{bf} + (n-1)\left(\varphi_{p1}k_{p1} + \varphi_{p2}k_{p2}\right) - (n-1)\varphi k_{bf} \right)}{\left(\frac{(\varphi_{p1}k_{p1}+\varphi_{p2}k_{p2})}{\varphi} + (n-1)k_{bf} - \left(\varphi_{p1}k_{p1} + \varphi_{p2}k_{p2}\right) + \varphi k_{bf} \right)} \tag{5}$$

$$\frac{\mu_{hnf}}{\mu_{bf}} = \left[\frac{1}{1 - 34.87 \times \left(d_f\right)^{0.3} \left(\left(d_{p1}\right)^{-0.3} (\varphi_1)^{1.03} + \left(d_{p2}\right)^{-0.3} (\varphi_2)^{1.03} \right)} \right] \tag{6}$$

4.1. Hydraulic diameter

Hydraulic diameter (d_h) depends on the variation of area and wetted perimeter, as it is directly related to the four times of the area and inversely related to the perimeter. However, in the current study, this approach was found to be ineffective as the cross-sectional area of channel varies along the length. To compute the hydraulic diameter for varying cross-sectional area, the technique presented by [29] has been adopted in this study. Chen et al. [29] numerically analyzed the hydrothermal performance of staggered ASPF and zigzag printed circuit heat exchangers. According to the results, ASPF offered better heat transfer characteristics with a slight increase in pressure drop. Cui et al. [30] also followed the same technique to compute the d_h of channels having airfoil shaped pin-fins. To define the d_h of studied configuration, specific section of heat sink is presented in Fig. 6. To obtain the d_h, the following set of equations were used Eqs. (2)–(4).

$$V_{fin} = (L \times W - A_{ss,top})H \tag{2}$$

$$A_{ss,\ side} = 2\left(P_{fin} \times H/2\right) + 2\left(L - L_{fin}\right)H + 2(L \times W - A_{ss,top}) \tag{3}$$

$$d_h = \frac{4V_{fin}}{A_{ss,\ side}} \tag{4}$$

where W, L, *and* H symbolized the width, length, and the specific section height while $A_{ss,top}$, V_{fin}, P_{fin}, $A_{ss,\ side}$, *and* L_{fin} denoted the top surface area, volume, perimeter, side surface area, and pin-fin length, respectively.

4.2. Thermophysical properties

Literature reports numerous studies that used the classical models developed by different investigators to compute nanofluids' thermophysical properties (heat capacity, viscosity, thermal conductivity, and density). The presented study employed the classical models of Hamilton–Crosser [49] and Corcione [50] to compute the thermal conductivity (k) and viscosity (μ), while the models of Xuan and Roetzel [51] and Pak and Cho [52] was used to evaluate the heat capacity (C_p) and density (ρ) of the prepared samples of nanofluid. Investigators used these models in different numerical and experimental studies [53–61].

The studies [62,63] used the extended forms of the classical models for estimating the thermophysical properties of hybrid nanofluids. The results revealed that at low particle concentration (≤ 0.1 $\%vol.$) these models can predict the values of thermal conductivity, viscosity, heat capacity and density with a slight deviation from the experimental results. However, the error was raised with an increase in particle concentration. Eqs. (5)–(8) provide the extended forms of the classical models of Hamilton–Crosser [49], Corcione [50], Xuan and Roetzel [51], and Pak and Cho [52] used for the calculation of thermal conductivity, viscosity, heat capacity, and density, respectively.

$$C_{p,hnf} = \left(\frac{\varphi_{p1}\rho_{p1}C_{p,p1} + \varphi_{p2}\rho_{p2}C_{p,p2} + (1-\varphi)\rho_{bf}C_{p,bf}}{\rho_{hnf}} \right) \tag{7}$$

$$\rho_{hnf} = \varphi_{p1}\rho_{p1} + \varphi_{p2}\rho_{p2} + (1-\varphi)\rho_{bf} \tag{8}$$

where k, d_f, φ, μ, ρ, n, d_p, $M, and\ N$ symbolized the thermal conductivity, base fluid molecule diameter, particle volume fraction, viscosity, density, empirical shape factor, particle diameter, molecular weight, and Avogadro's number, respectively. Whereas, the subscripts p, bf, and hnf denoted the nanoparticle, base fluid, and hybrid nanofluid, respectively.

4.3. Performance parameters

To compute the hybrid nanofluid thermophysical properties, mean bulk temperature was used calculated using Eq. (9).

$$T_{mean} = \frac{T_{inlet} + T_{outlet}}{2} \tag{9}$$

The rate of heat transfer ($\dot{Q}$) between the coolant flowing inside the channels and heat sink is computed using Eq. (10).

$$\dot{Q} = \dot{m}C_p(T_{outlet} - T_{inlet}) \tag{10}$$

where C_p and $\dot{m}$ denoted the heat capacity mass flow rate of the flowing fluid, respectively.

Thermocouples were installed just below the channel wall to record the temperature values. Eq. (11) was used to calculate channel wall temperature.

$$T_w = T_b - \left(\frac{Q l_w}{k_s A_w} \right) \tag{11}$$

where l_w denoted the base to channel wall surface distance that was 2 mm in the current study while, k_s and A_w symbolized the heat sink thermal conductivity and wall surface area. The wall surface area was determined by Eq. (12).

$$A_w = L_s \times W_s \tag{12}$$

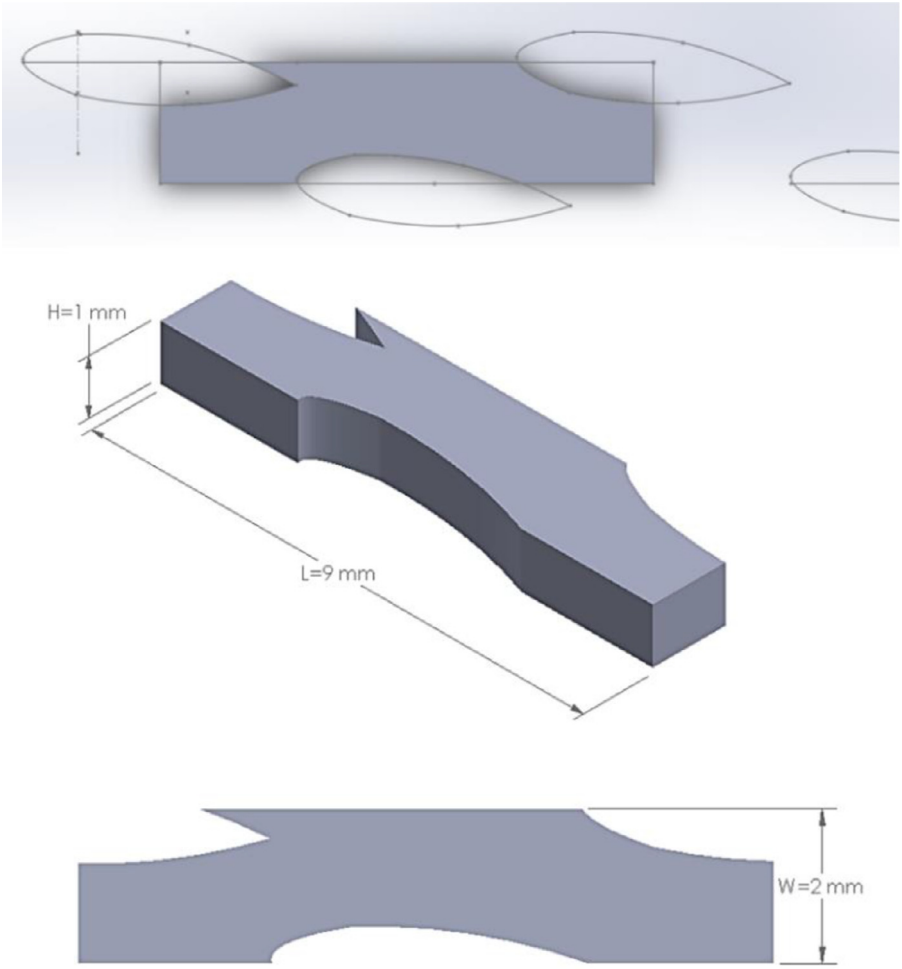

Fig. 6. Specific section of staggered oriented airfoiled shaped pin fin configuration.

where W_s and L_s represented the width and length of the under-consideration part of heat sink.

Logarithmic mean temperature difference ($LMTD$) and convective heat transfer coefficient (h) was evaluated using Eqs. (13) and (14), respectively.

$$LMTD = \frac{(T_w - T_{inlet}) - (T_w - T_{outlet})}{\ln\left[\frac{(T_w - T_{inlet})}{(T_w - T_{outlet})}\right]} \tag{13}$$

$$h = \left[\frac{mC_p(T_{outlet} - T_{inlet})}{A_{seff} \times (LMTD)}\right] \tag{14}$$

where A_{seff} symbolized the sink effective area.

Reynolds number (Re) was calculated using Eq. (15).

$$Re = \frac{\rho v d_h}{\mu} \tag{15}$$

To compute the average fluid velocity and channel average cross-sectional area Eqs. (16) and (17) was used, respectively.

$$v = m/A_{avg.} \tag{16}$$

$$A_{avg.} = \frac{V_{fin}}{L} \tag{17}$$

Thermal resistance (R_{th}) was evaluated by Eq. (18), while Nusselt number (Nu) was computed using Eq. (19).

$$R_{th} = \frac{LMTD}{\dot{Q}} \tag{18}$$

$$Nu = \frac{hd_h}{k_c} \tag{19}$$

where k_c symbolized the thermal conductivity of flowing fluid (coolant).

To compute the pumping power (PP) Eq. (20) has been used.

$$PP = V \times \Delta P \tag{20}$$

where ΔP and V represented the pressure drop across the test section and volumetric flow rate, respectively.

4.4. Uncertainty analysis

Uncertainty analysis is essential for micro or mini scale experiments to provide the best demonstration of experimental results errors associated with measuring instruments needed to be carefully examined. To compute the uncertainty in different measuring parameters, presented study adopted the same technique followed by different investigators [32,35]. The following set of Eqs. (21)–(25) provides the uncertainties (ε) in Reynolds number, heating power, convective heat transfer coefficient, Nusselt number, and pressure drop, respectively. Maximum values of uncertainty for Nusselt number, pressure drop, and the Reynolds number was never found to be more than 6.79%, 0.81%, and 2.185%, respectively.

$$\varepsilon_{Re} = \frac{U_{Re}}{Re} = \sqrt{\left(\frac{U_\rho}{\rho}\right)^2 + \left(\frac{U_{\bar{V}}}{\bar{V}}\right)^2 + \left(\frac{U_\mu}{\mu}\right)^2} \tag{21}$$

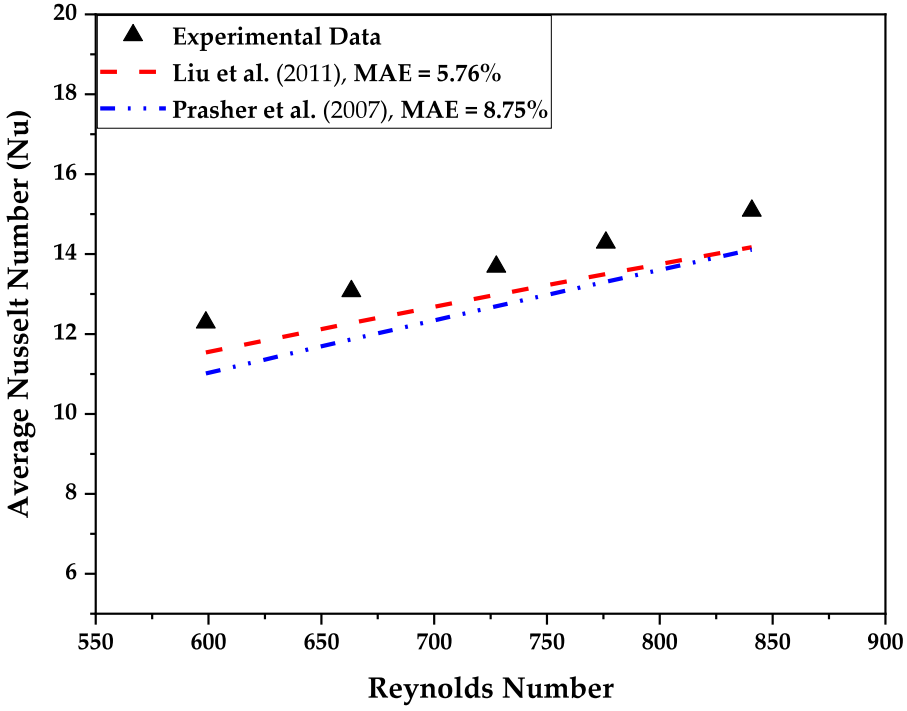

Fig. 7. Comparison of experimental data with the models of Liu et al. [64] and Prasher et al. [65].

$$\varepsilon_Q = \frac{U_Q}{Q} = \sqrt{\left(\frac{U_V}{V}\right)^2 + \left(\frac{U_I}{I}\right)^2} \tag{22}$$

$$\varepsilon_h = \frac{U_h}{h} = \sqrt{\left(\frac{U_Q}{Q}\right)^2 + \left(\frac{U_{(T_w-T_i)}}{(T_w-T_i)}\right)^2 + \left(\frac{U_{(T_w-T_o)}}{(T_w-T_o)}\right)^2 + \left(\frac{U_\rho}{\rho}\right)^2 + \left(\frac{U_{C_p}}{C_p}\right)^2 + \left(\frac{U_{A_b}}{A_b}\right)^2 + \left(\frac{U_\nu}{\nu}\right)^2 + \left(\frac{U_{(T_{out}-T_{in})}}{(T_{out}-T_{in})}\right)^2} \tag{23}$$

$$\varepsilon_{Nu} = \frac{U_{Nu}}{Nu} = \sqrt{\left(\frac{U_h}{h}\right)^2 + \left(\frac{U_k}{k}\right)^2 + \left(\frac{U_{D_h}}{D_h}\right)^2} \tag{24}$$

$$\varepsilon_{\Delta P} = \sqrt{\left(\frac{U_{\Delta P}}{\Delta P}\right)^2} \tag{25}$$

5. Results and discussion

5.1. Validation

To validate the experimental configuration, authors compared the experimental data of staggered oriented ASPFHS with the derived models of Liu et al. [64] and Prasher et al. [65] using water as a cooling agent and varying *Re* from 600 to 850. The results revealed that experimental data showed a good agreement with the models of Prasher et al. [65] and Liu et al. [64], represented with Eqs. (26) and (27). Liu et al. [64] performed an experimental investigation on the augmentation of *Nu* varying *Re* in the range of (60-800). The study was conducted on the square shaped pin-fin heat sink with de-ionized water as a coolant. The researchers noticed an increase in *Nu* with the increase in *Re* and proposed a model on the basis of experimental results to predict the average *Nu*. Prasher et al. [65] analyzed the hydrothermal performance of staggered circular and square shaped pin-fins heat sink in the LFR ($Re = 40 - 1000$). The work was done by varying the flow of water in circulation through the mico-channels of the heat sink and proposed a correlation for the prediction of the average *Nu*. The friction factor (*f*) was calculated using Eq. (28) to validate the pressure drop measurements [66], and compared to the value estimated using the Gunther and Shaw [67] correlation, Eq. (29). Mean absolute error (MAE) is computed using Eq. (30) to examine the deviation of experimental results from the predicted values of models. It has been noticed that the presented models of Liu et al. [64], Prasher et al. [65], and Gunther and Shaw [67] predicted the experimental results obtained in this study with a MAE of 5.76%, 8.75%, and 11.9% respectively, as shown in Figs. 7 and 8.

$$Nu = 0.281\ Re^{0.73} \left(\frac{S_L - d_f}{d_f}\right)^{-0.63} \tag{26}$$

$$Nu = 0.1245\ Re^{0.6106}\ Pr^{0.36} \left(\frac{Pr}{Pr_s}\right)^{0.25} \tag{27}$$

$$f = \frac{\Delta P}{n\rho.\frac{v^2}{2}} \tag{28}$$

$$f = \frac{180}{Re} \left(\frac{4S_tS_L}{\pi d_f} - 1\right)^{0.4} \left(\frac{S_L}{S_t}\right)^{0.6} \tag{29}$$

$$\text{Mean Absolute Error} = \text{MAE} = \frac{1}{N}\sum_{j=1}^{N}\left[\frac{\left|U_{exp.} - U_{pred.}\right|}{U_{exp.}}\right] \tag{30}$$

where $d_f, S_L, S_t, Pr_s, h_f, dh, h_c, n, U_{pred.}, U_{exp.}$, *and* N are symbolized the hydraulic diameter of fin, longitudinal pitch, transverse pitch, Prandtl number at the surface, fin height, channel clearance,

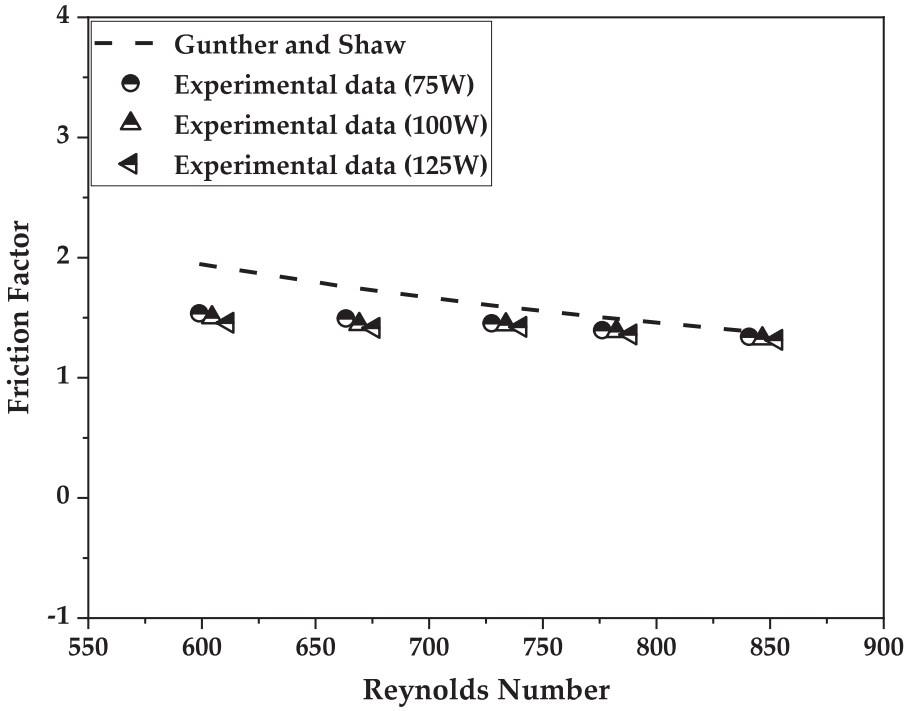

Fig. 8. Comparison of experimental friction factor values with the estimated values of Gunther and Shaw [67] correlation.

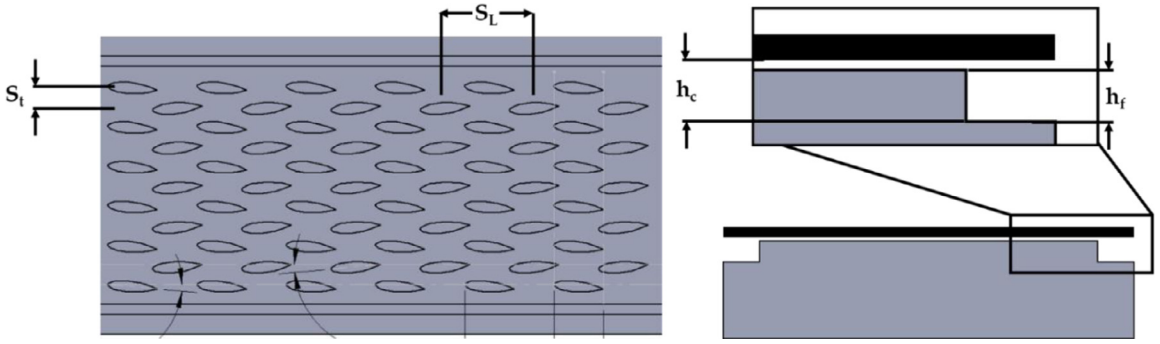

Fig. 9. Clarification of the channel clearance, longitudinal and transverse pitch (channel top and side view).

height of channel, number of pin-fin rows, predicted quantity, experimental quantity, and number of data points, respectively. Fig. 9 illustrates the channel clearance with a magnifying view, while the top view clarifies the longitudinal and transverse pitch.

5.2. Nusselt number

As shown in Fig. 10, the Nusselt number acquired to be improved with increasing flow or Reynolds number and heating power of water. The same trend was observed for the cases of all hybrid nanofluids (25:75, 50:50, 75:25). It was revealed that the nanofluid having mixture ratio of 50:50 delivered better results than others at all heating powers as shown in Fig. 11. Thermal conductivity of ferric oxide is higher than that of silica that is the reason of this enhancement in heat transfer rate for the mixture ratio of 50:50. In addition, it was revealed that mixture ratio having more than 50% ferric oxide showed diminution in results. Minimum enhancement in Nusselt number was observed for hybrid nanofluid (Fe_2O_3-SiO_2) having mixture ratio of (75:25). It may be due to stability issues, larger particle size and density values of Fe_2O_3 nanoparticles which made the particles suspension nonuniform. The size of nanoparticles contributed well to the variation of heat transfer rate of working fluid [68]. The size of SiO_2 nanoparticles that is 20nm, almost half size of the particles of ferric oxide. According to the results, the augmentation and diminution of Nusselt number depend upon the individual particle advantages and disadvantages trade-off.

Fig. 11(d) provides the graphical illustration of average enhancement in Nusselt number in comparison of water. The maximum improvement in Nusselt number was found at 75W, followed by 100W and 125W. Some of the recent studies also observed the same effect [69,70] and stated that it was due to the particle's instability in fluid, with the increase in heating power fluid temperature raised which subsequently deteriorated the effect of surfactant and caused the instability of suspended nanoparticles.

5.3. Wall temperature

As anticipated, the nanoparticle suspension increased the rate of heat transfer between the coolant (water or nanofluid) and the sink wall, resulting in a decrease in wall temperature compared to the base fluid. The noticeable diminution in wall temperature was observed at all mixture ratios and a decreasing trend with *Re*. Maximum *Nu* was found for the fluid having an equal percentage

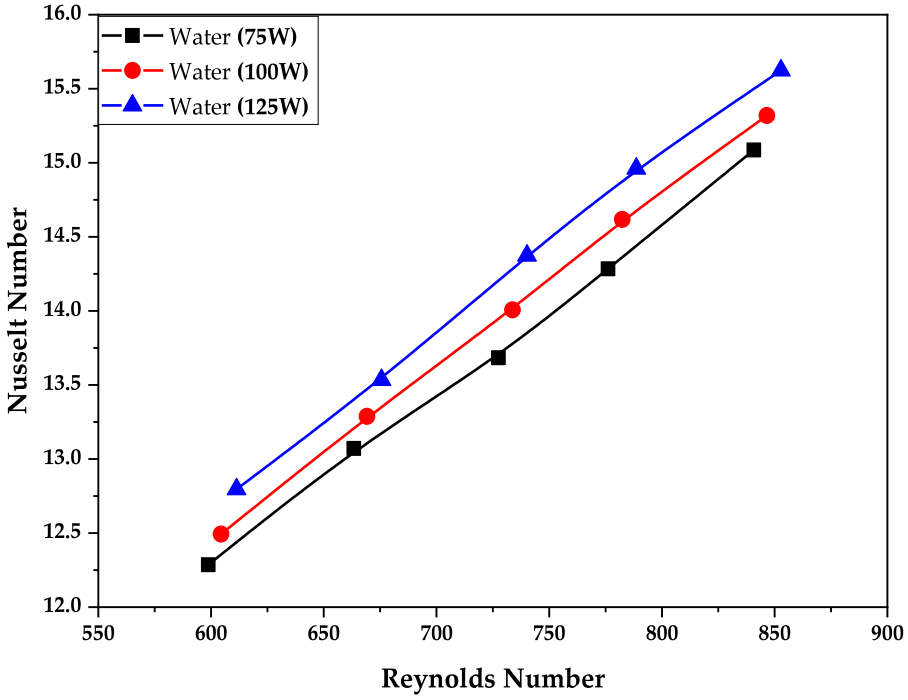

Fig. 10. Variation of Nusselt number of distilled water against Reynolds number at different heating powers.

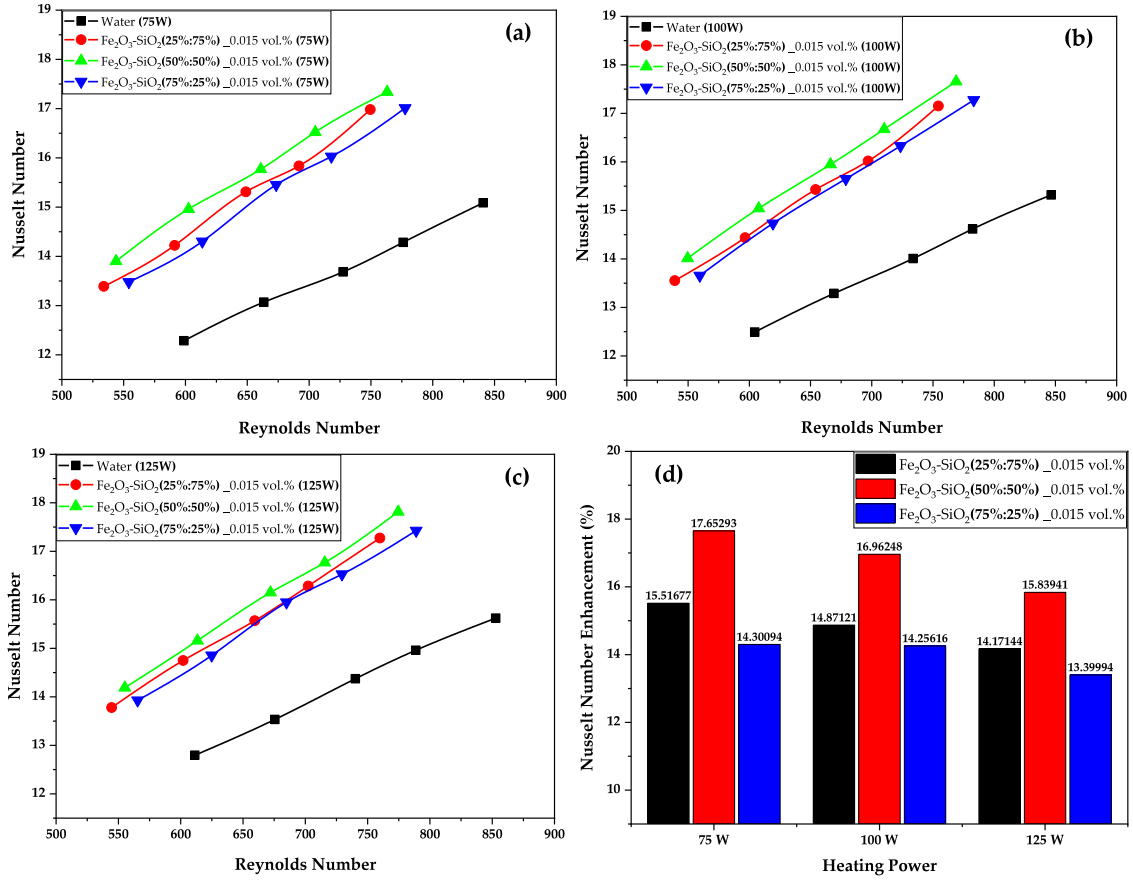

Fig. 11. Variation of Nusselt number of all three mixture ratios of hybrid nanofluid and distilled water against Reynolds number.

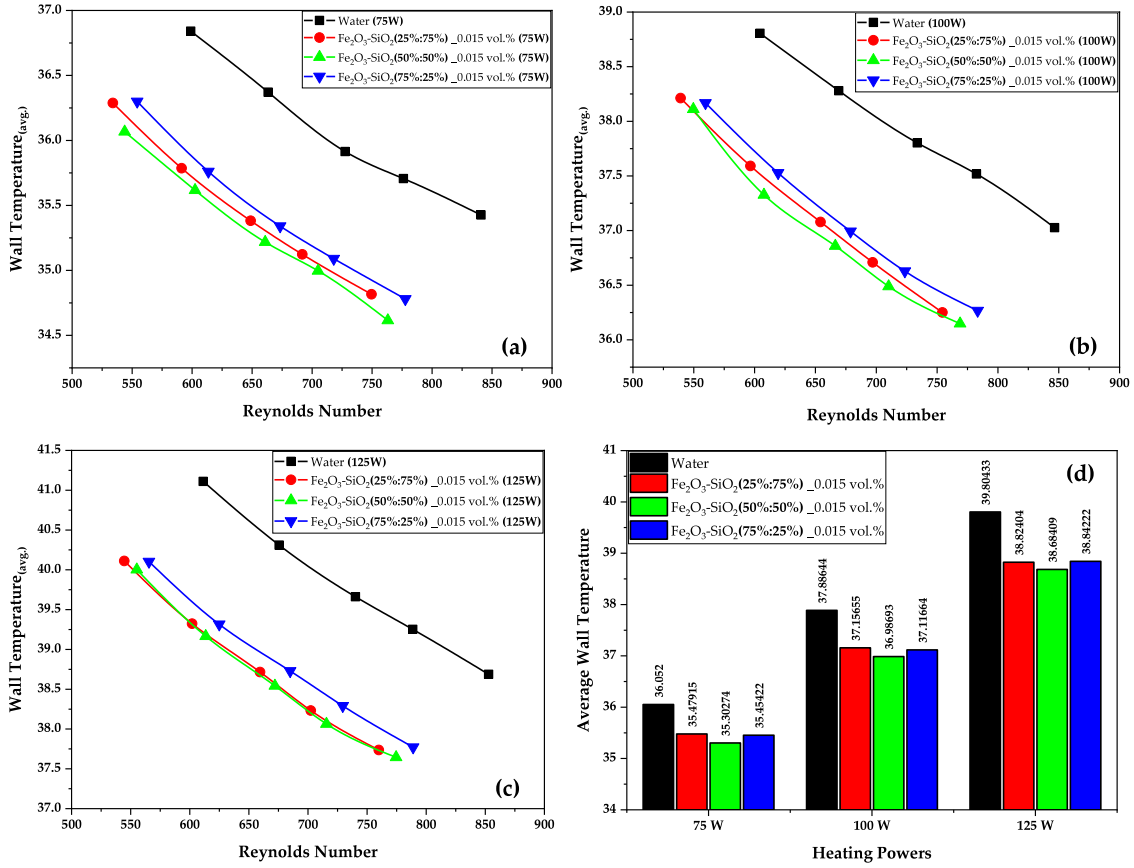

Fig. 12. Variation in average wall temperature against Reynolds number for water and hybrid nanofluid at different heating powers.

of nanofluid (50:50), thus the wall temperature for this mixture ratio was minimal.

The interaction between the particles and with the walls of heat sink caused the augmentation of heat transfer and reduction in wall temperature for the case of nanofluid. Fig. 12 demonstrated the wall temperature variation for water and different hybrid nanofluid at 75 W, 100 W, and 125 W, respectively. In addition, the average wall temperatures of water and nanofluid at different heating powers are graphically illustrated in Fig. 12(d).

5.4. Thermal resistance

Thermal resistance of hybrid nanofluid was found to be reduced as the rate of heat transfer increased with the suspension of metallic oxide nanoparticles—thermal resistance and heat transfer rate interrelated with each other inversely. So, the same trend was observed for thermal resistance as the Nusselt number but in a reversed manner. The nanofluid having equal percentages of ferric oxide and silica showed the least thermal resistance in comparison of other mixture ratios. Fig. 13 represented the variation in thermal resistance of water and hybrid nanofluids having different mixture ratios at 75 W, 100 W, and 125 W, respectively.

Fig. 13(d) provides the graphical illustration of the minimal thermal resistance values obtained at maximum Reynolds number for water and hybrid nanofluids having mixture ratios of (25:75, 50:50, 75:25) at different heating powers. The minimum values of thermal resistance were found at 75 W due to the maximum enhancement of Nusselt number followed by 100 W and 125 W.

5.5. Pumping power

The size and density of particles significantly affected the pumping power. Investigators observed an enhancement in viscosity of fluid with the suspension of nanoparticles [71,72]. The influence of particle size on the viscosity of nanofluid is inconclusive, some studies observed an enhancement in viscosity of nanofluid with the increase in particles diameter [73–75], while few reported contradictory results [76,77]. As expected, a noticeable increase in *PP* was observed with the increase in Reynolds number and the addition of nanoparticles for all studied mixture ratios, graphically represented with Fig. 14(a). A slight decrease in pumping power was also observed increasing the heating power, Fig. 14(b). In addition, increasing the percentage of silica nanofluid resulted in a slight increase in pumping power. Higher viscosity due to a smaller size and greater number of particles of SiO_2 at a particular concentration than that of Fe_2O_3 could be the possible reasons for this increase in pumping power [78]. Little variation in pumping power was observed in comparison of nanofluids because the other factors such as the larger particle size of ferric oxide (almost two times greater), greater density values, and stability also influenced the results. However, the effect may be different for the combination of ferric oxide with other nanoparticles.

5.6. Repeatability

Repeatability is important in experimental studies conducted on nanofluids to ensure stability and reliability, it was observed that after a certain time, the sedimentation of nanoparticles began that caused the diminution in *Nu* and augmented the pumping power. Authors tested the prepared samples of ferric oxide-silica hybrid nanofluid after 12h and compared the results with the study car-

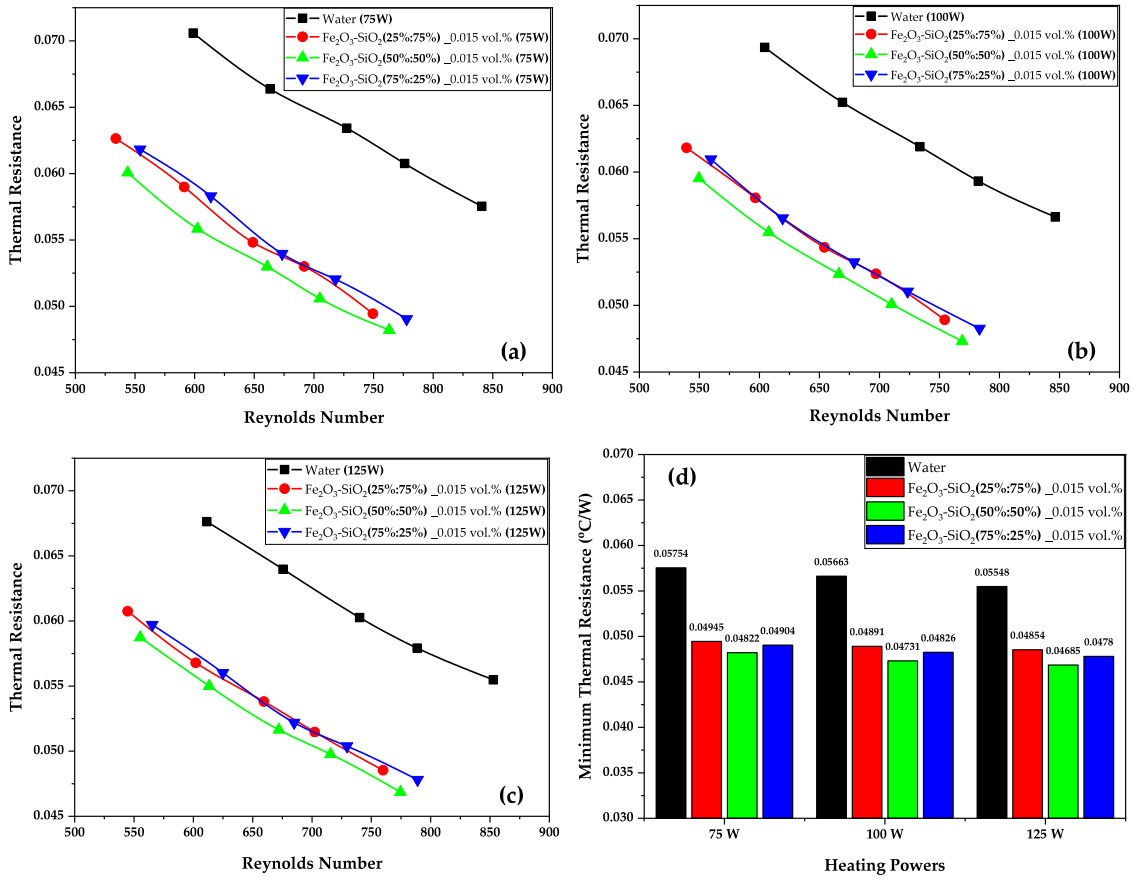

Fig. 13. Diminution of thermal resistance for water and nanofluid (Fe_2O_3-SiO_2) with Reynolds number at different heating powers.

ried out just after the sonication and stirring. According to the results, the repeated data were very close to the experimental values acquired just after preparation that ensured the stability of prepared samples, as shown in Fig. 15. Results showed good repeatability with a maximum deviation of 1.02% and 1.58% for pumping power and *Nu*.

5.7. Comparison of results

The sole purpose of comparing the experimental results with different geometrical configurations is to highlight the significance of airfoil shaped pin-fins as it has been observed that airfoil shaped pin-fin offered excellent effective surface providing less flow resistance. As expected, the presented study offered remarkable results. In comparison of most of the recently studied geometrical configurations, the geometrical configuration investigated in current study exhibited a better rate of heat transfer with a little penalty of pressure drop. Figs. 16 and 17 graphically illustrate the pressure drop and average Nusselt number comparison of the oriented airfoil pin-fin geometrical configuration with different sink configurations. Azizi et al. [79] experimentally examined the pressure drop and heat transfer variation inside a cylindrically shaped mini channel heat sink having hydraulic diameter 560 μm. The study was carried out by varying the *Re* in the LFR ($Re < 900$). According to the results, a significant increase in pressure drop and heat transfer coefficient was found with the increase in Reynolds number.

Esmaili et al. [80] studied the effect of rib angles (30°, 45°, 60°, 90°) on the hydrothermal performance of rectangular shaped micro-ribbed (height = 100 μm) heat sink in the LFR ($184 < Re <$ 1800). It was found that the angled ribs delivered the better results while heat sink with 45° rib angle showed best thermal performance among all tested geometries. However, pressure drop was found to enhance in the following sequence (45°>30°>60°>90°). According to Hassani et al. [81], the heat transport characteristics of heat sink can be augmented with the insertion of interruptions. Investigators analyzed the effect of seven different types of interruptions in fluid flow channels and observed a significant improvement in heat transfer with a small pumping power penalty. A maximum of 10% reduction in fin surface temperature was observed at a Reynolds number of 900.

Khoshvaght-Aliabadi et al. [82] evaluated the hydraulic and thermal performance of sinusoidal, trapezoidal, and triangular shaped plate-pin fin and plate fin corrugated miniature heat sink varying Reynolds number (100-900). It was observed that the heat sink having plate-pin fin showed better thermal performance and less pressure loss compared to plate fin heat sink. The study conducted by Ahammed et al. [83] on multiport mini-channel heat sink observed an increase in pressure drop with increased Reynolds number. Arshad and Ali [55] observed the variation of pressure drop with heating power in a rectangular shaped mini-channel heat sink. The results showed a significant decrease in the pressure drop with an increase in the heating power. A diminution of almost 11.35% in pressure drop was found by increasing the heating power from 100W to 150W. Ali and Arshad [84] compiled an experimental study to analyze the effect of fins positioning on the thermal characteristics of square shaped pin-fin heat sink. According to the results, staggered pin-fin geometrical configuration showed a better heat transfer rate in comparison of inline configuration. Khoshvaght-Aliabadi et al. [85] examined the MCHS having

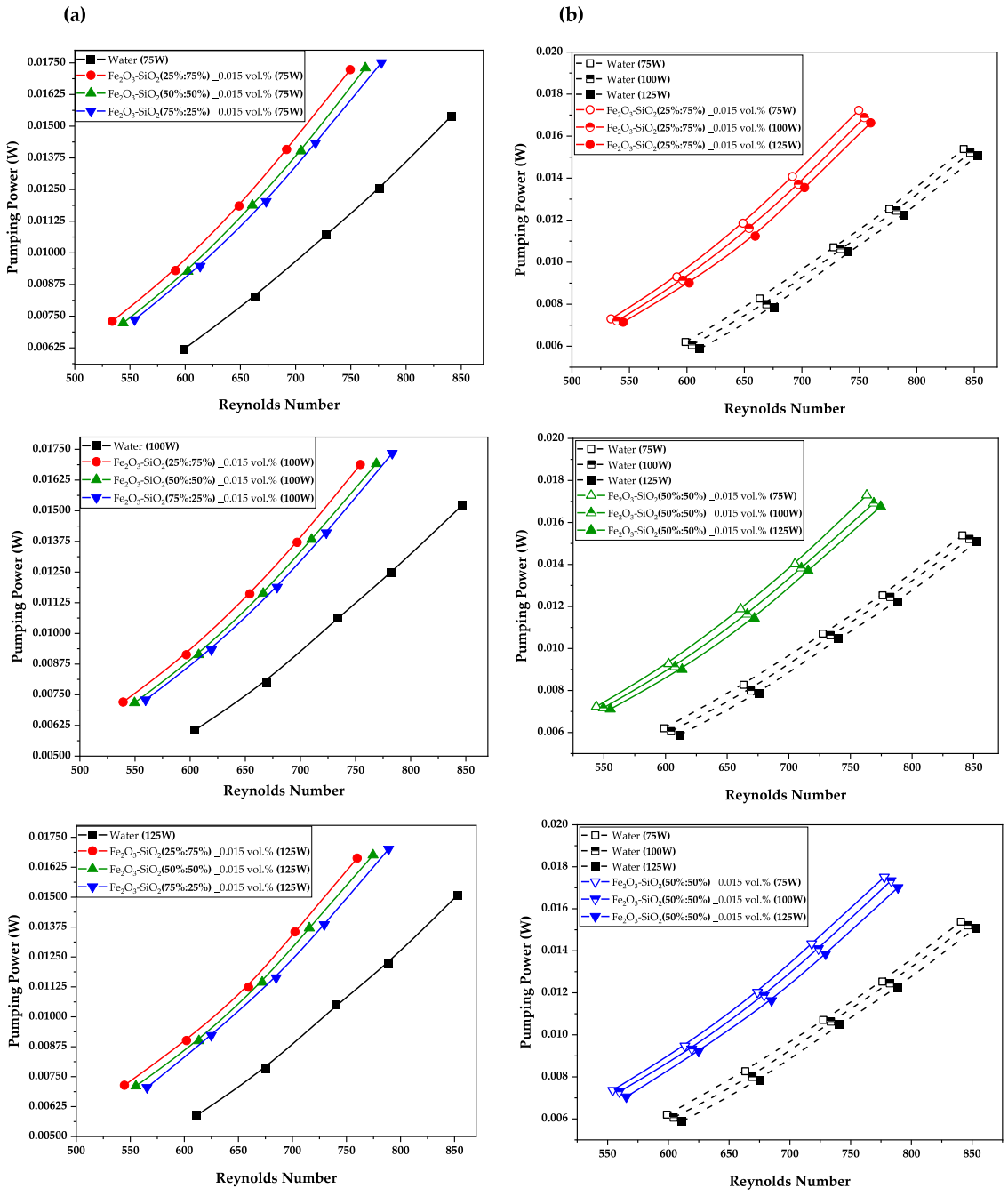

Fig. 14. Pumping power variation of (a) different fluids at same heating powers, (b) each fluid at various heating powers, against the Reynolds number.

different nook configurations (circular, triangular, and rectangular). It was observed that non-flat nooks sink configurations showed better thermal performance with a little penalty of pressure drop.

According to Xia et al. [86], the addition of ribs in straight channels significantly enhanced the Nusselt number. Chai et al. [87] studied the interrupted channel and interrupted channel in combination with ribs. Interestingly, it was found that for Reynolds number below 600, the heat sink having interrupted channel in combination with ribs showed better results, while for $Re > 600$ channels without ribs exhibited better Nusselt number. Sajid et al. [69] studied the wavy-shaped mini-channel heat sink varying the channel wavelength, channel width, and flowrate. Investigators observed a notable effect of channel width and wavelength on heat transfer rate, while the effect of channel width was found to be more significant than that of channel width. Ambreen and Kim [88] numerically analyzed the square, circular, and hexagonal shaped pin-fin heat sinks under identical flow conditions. The results revealed that the circular shaped pin fins exhibited better heat transfer characteristics, followed by geometric configurations of hexagonal and square shape. According to the investigators, it was because of the delayed separation of flowing fluid at the rear end that caused the uniform flow distribution. The study conducted by Sui et al. [89] observed that the sinusoidal shaped mini-channel heat sink offered much better heat transfer as compared to straight channels. In addition, the penalty of pressure

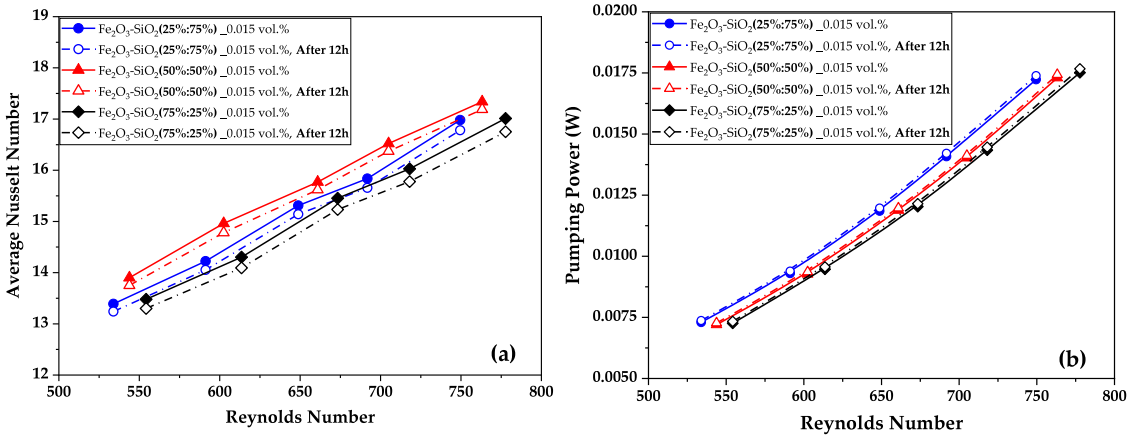

Fig. 15. Repeatability test for Nusselt number and pumping power employing hybrid nanofluid of ferric oxide-silica hybrid nanofluid.

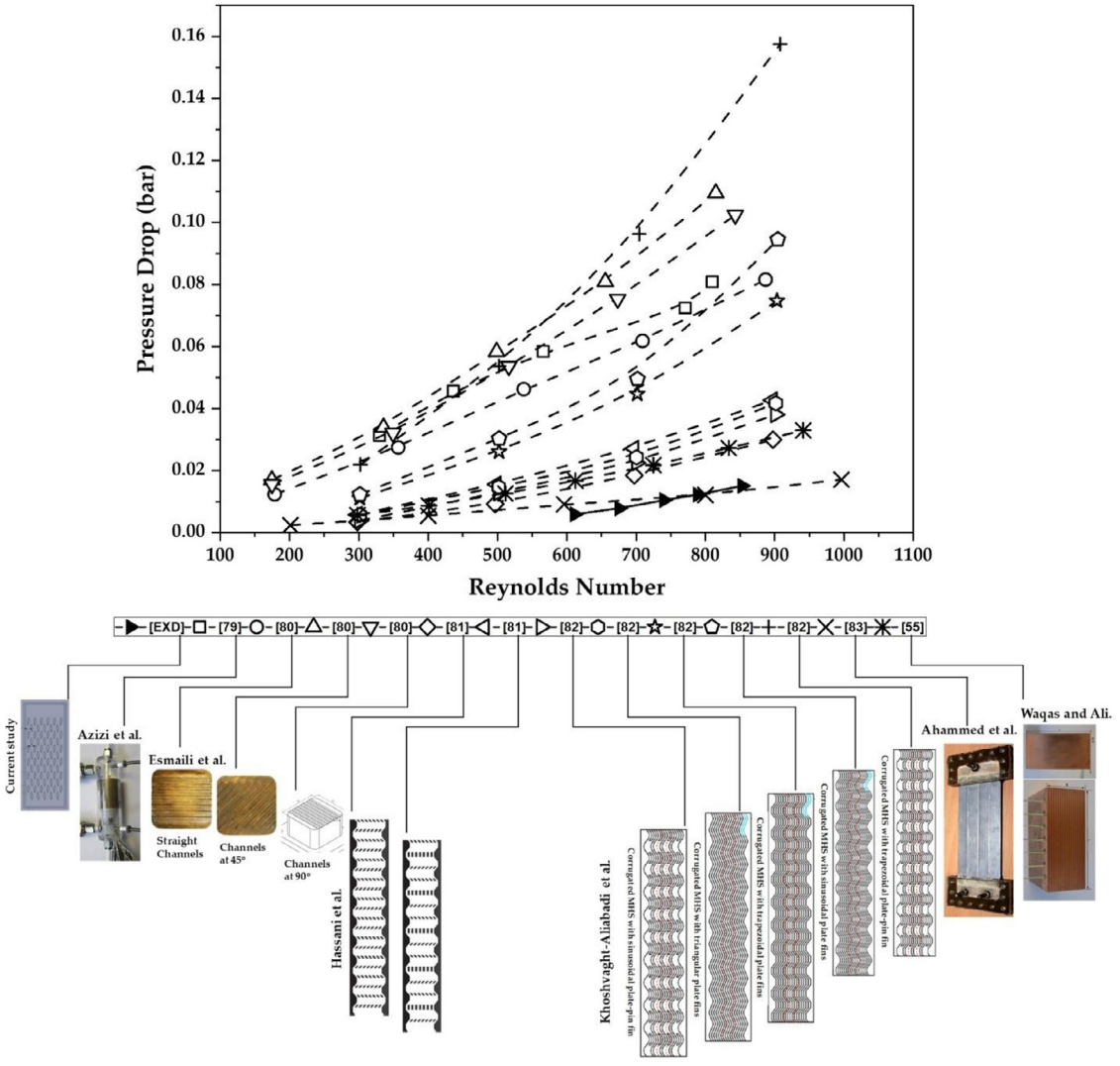

Fig. 16. Pressure drop comparison of experimental data with the recently published studies on heat sinks having different geometrical configurations using water as a coolant.

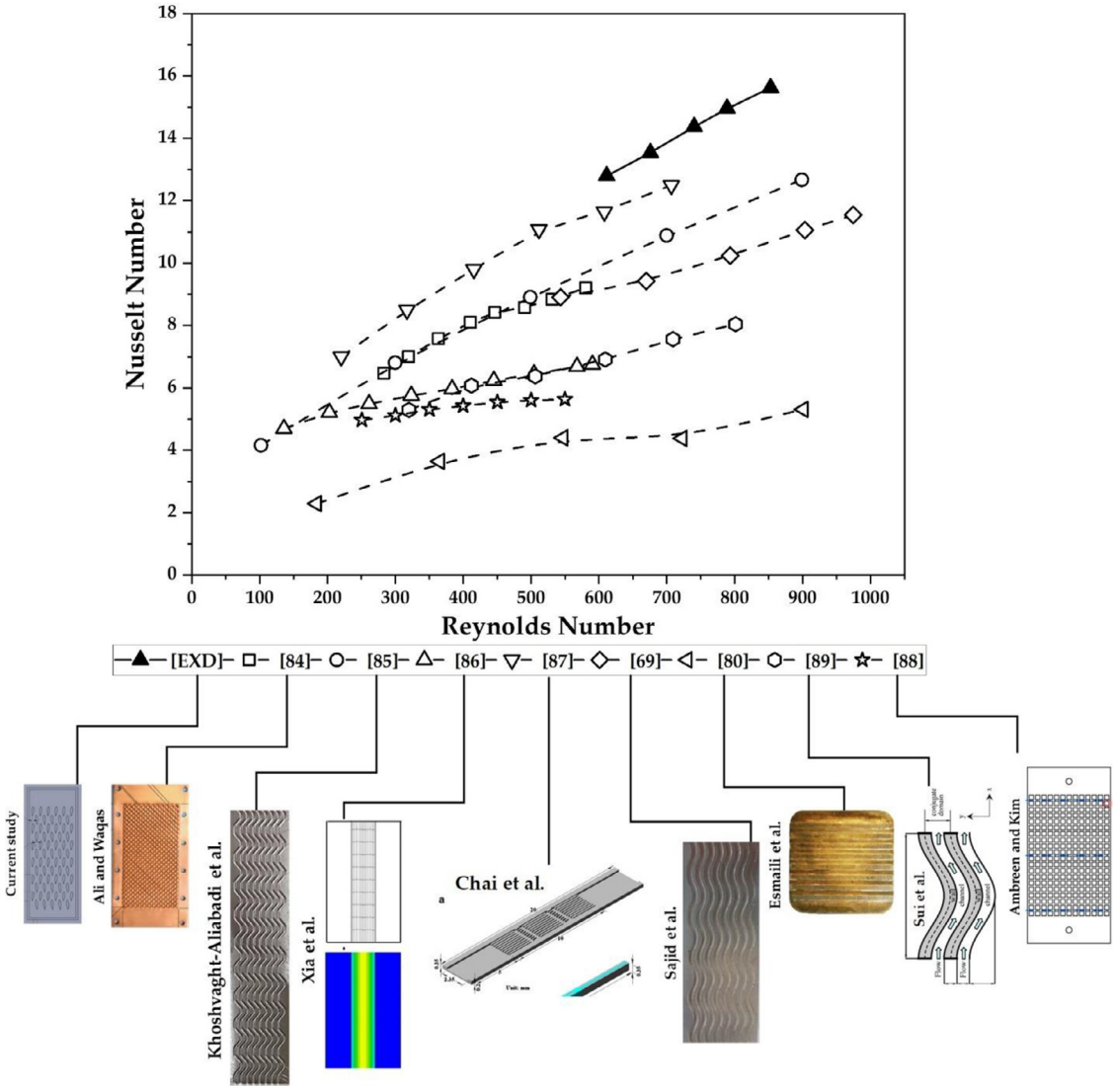

Fig. 17. Nusselt number comparison of experimental data with the recently published studies on heat sinks having different geometrical configurations using water as a coolant.

drop was also found to be much smaller than that of heat transfer augmentation.

6. Concluding remarks and future recommendations

The presented study experimentally studied the hydrothermal performance of staggered oriented pin-fin heat sink employing the novel hybrid nanofluid of ferric oxide-silica/water with different mixture ratios (25:75, 50:50, 75:25). The results were analyzed at various flow rates and heating powers. On the basis of obtained results, the following deductions were made:

- Commendable results were observed with the implementation of hybrid nanofluids of (Fe_2O_3-SiO_2/water) having different mixture ratios (25:75, 50:50, 75:25). Enhancement in Nusselt number and pumping power was obtained at all mixture ratios, however, the impact of different mixture ratios was different on the results.
- Hybrid nanofluid of (Fe_2O_3-SiO_2) with equal volume fraction was found to be the best of all mixing ratios studied. Maximum augmentation of 15.52%, 17.65%, and 14.3% in Nusselt number for the mixture ratios of 25:75, 50:50, and 75:25 was achieved at 75W.
- The Nusselt number was found to increase with the Reynolds number, while a slight decrease was observed with the increase in heating power.
- In comparison to water, all hybrid nanofluid samples exhibited a considerable enhancement in pumping power. Furthermore, it was revealed that the pumping power increased with the silica nanofluid mixing ratio. The other important factor observed during the experimental study concerned the improvement of pumping power with flow rate. It was noticed that as the flow rate increased, the enhancement in pumping power between the nanofluids with different mixture ratios increased.

The key findings of this experimental work will be beneficial to advance towards the highly efficient heat sinks for electronic cooling or to use in different application areas. Researchers have much to do in this arena, including:

- Investigate the hydrothermal performance with different unitary and hybrid nanofluids and draw a comparative study to

find out the one that suits best for heat sink having airfoil pin fins.
- It would be a significant contribution to develop empirical correlation of Nusselt number and friction factor for airfoil fin heat sink considering peripheral area of pin fins, longitudinal and transverse distance between fins, fins orientation, fin height, hydraulic diameter, Prandtl number, and Reynolds number.
- Alterations in geometrical configurations such that fins positioning and orientation could be very helpful to augment the heat transfer rate offering a slight increase in pumping power.
- Presented study was conducted at lower particle concentration due to the stability issues, these configurations may perform differently (either improve or deteriorate the balance of thermal and hydrodynamic performance) at high concentrations >0.1 vol.%.
- The penalty of pumping power and flow resistance can be reduced by coating the channels with hydrophobic and superhydrophobic materials, however, it is effective at lower pumping power [90,91].

Authors' statement

Hamza Babar: Experimental Design; Methodology; Validation; Analysis; Draft writing. **Hongwei Wu:** Conceptualization; Supervision. **Hafiz Muhammad Ali:** Conceptualization; Supervision. **Tayyab Raza Shah:** Setup preparation. **Wenbin Zhang:** Final Draft; Discussion

Declaration of Competing Interest

We declare that we have no financial and personal relationships with other people or organizations that can inappropriately influence our work, there is no professional or other personal interest of any nature or kind in any product, service and/or company that could be construed as influencing the position presented in, or the review of, the manuscript entitled "Staggered oriented airfoil shaped pin-fin heat sink: Investigating the efficacy of novel water based ferric oxide-silica hybrid nanofluid".

References

[1] H. Babar, H.M. Ali, Towards hybrid nanofluids: preparation, thermophysical properties, applications, and challenges, J. Mol. Liq. 281 (2019) 598–633, doi:10.1016/j.molliq.2019.02.102.

[2] H. Maleki, M.R. Safaei, A.S. Leon, T. Muhammad, T.K. Nguyen, Improving shipboard electronics cooling system by optimizing the heat sinks configuration, J. Ocean Eng. Sci. (2021), doi:10.1016/j.joes.2021.09.013.

[3] M.A. Hayat, Y. Chen, M. Bevilacqua, L. Li, Y. Yang, Characteristics and potential applications of nano-enhanced phase change materials: A critical review on recent developments, Sustain. Energy Technol. Assess. 50 (2022) 101799, doi:10.1016/j.seta.2021.101799.

[4] M. Bahiraei, S. Heshmatian, M. Goodarzi, H. Moayedi, CFD analysis of employing a novel ecofriendly nanofluid in a miniature pin fin heat sink for cooling of electronic components: effect of different configurations, Adv. Powder Technol. 30 (2019) 2503–2516, doi:10.1016/j.apt.2019.07.029.

[5] S. Anitha, M.R. Safaei, S. Rajeswari, M. Pichumani, Thermal and energy management prospects of γ-AlOOH hybrid nanofluids for the application of sustainable heat exchanger systems, J. Therm. Anal. Calorim. 147 (2022) 6941–6957, doi:10.1007/s10973-021-10996-9.

[6] H. Abbassi, C. Aghanajafi, Evaluation of heat transfer augmentation in a nanofluid-cooled microchannel heat sink, J. Fusion Energy 25 (2006) 187–196, doi:10.1007/s10894-006-9021-x.

[7] X. Wu, H. Wu, P. Cheng, Pressure drop and heat transfer of Al2O3-H2O nanofluids through silicon microchannels, J. Micromech. Microeng. 19 (2009), doi:10.1088/0960-1317/19/10/105020.

[8] H.A. Mohammed, P. Gunnasegaran, N.H. Shuaib, Heat transfer in rectangular microchannels heat sink using nanofluids, Int. Commun. Heat Mass Transf. 37 (2010) 1496–1503, doi:10.1016/j.icheatmasstransfer.2010.08.020.

[9] M.A. Alazwari, M.R. Safaei, Non-isothermal hydrodynamic characteristics of a nanofluid in a fin-attached rotating tube bundle, Mathematics 9 (2021) 1153, doi:10.3390/math9101153.

[10] A. Moghadassi, E. Ghomi, F. Parvizian, A numerical study of water based Al2O3 and Al2O3–Cu hybrid nanofluid effect on forced convective heat transfer, Int. J. Therm. Sci. 92 (2015) 50–57, doi:10.1016/j.ijthermalsci.2015.01.025.

[11] A.N. Al-Shamani, K. Sopian, H.A. Mohammed, S. Mat, M.H. Ruslan, A.M. Abed, Enhancement heat transfer characteristics in the channel with trapezoidal rib-groove using nanofluids, Case Stud. Therm. Eng. 5 (2015) 48–58, doi:10.1016/j.csite.2014.12.003.

[12] R. Nimmagadda, K. Venkatasubbaiah, Conjugate heat transfer analysis of micro-channel using novel hybrid nanofluids (Al2O3 + Ag /Water), Eur. J. Mech. 52 (2015) 19–27, doi:10.1016/j.euromechflu.2015.01.007.

[13] W. Duangthongsuk, S. Wongwises, An experimental study on the thermal and hydraulic performances of nanofluids flow in a miniature circular pin fin heat sink, Exp. Therm Fluid Sci. 66 (2015) 28–35, doi:10.1016/j.expthermflusci.2015.02.008.

[14] A. Abdollahi, H.A. Mohammed, S.M. Vanaki, A. Osia, M.R. Golbahar Haghighi, Fluid flow and heat transfer of nanofluids in microchannel heat sink with V-type inlet/outlet arrangement, Alex. Eng. J. 56 (2017) 161–170, doi:10.1016/j.aej.2016.09.019.

[15] F. Zhou, I. Catton, Numerical evaluation of flow and heat transfer in plate-pin fin heat sinks with various pin cross-sections, Numer. Heat Transf. 60 (2011) 107–128, doi:10.1080/10407782.2011.588574.

[16] J.Y. Ho, K.K. Wong, K.C. Leong, T.N. Wong, Convective heat transfer performance of airfoil heat sinks fabricated by selective laser melting, Int. J. Therm. Sci. 114 (2017) 213–228, doi:10.1016/j.ijthermalsci.2016.12.016.

[17] C.-Y. Zhu, Y. Guo, H.-Q. Yang, B. Ding, X.-Y. Duan, Investigation of the flow and heat transfer characteristics of helium gas in printed circuit heat exchangers with asymmetrical airfoil fins, Appl. Therm. Eng. 186 (2021) 116478, doi:10.1016/j.applthermaleng.2020.116478.

[18] T.J. Praisner, E. Allen-Bradley, E.A. Grover, D.C. Knezevici, S.A. Sjolander, Application of nonaxisymmetric endwall contouring to conventional and high-lift turbine airfoils, J. Turbomach. (2013), doi:10.1115/1.4024023.

[19] T. Yavuz, E. Koç, Performance analysis of double blade airfoil for hydrokinetic turbine applications, Energy Convers. Manage. 63 (2012) 95–100, doi:10.1016/j.enconman.2012.01.032.

[20] M.H. Mohamed, G. Janiga, E. Pap, D. Thévenin, Multi-objective optimization of the airfoil shape of wells turbine used for wave energy conversion, Energy (2011), doi:10.1016/j.energy.2010.10.021.

[21] Q.F. Li, H. Quan, R.N. Li, D.J. Jiang, Influences of guide vanes airfoil on hydraulic turbine runner performance, Proc. Eng. (2012), doi:10.1016/j.proeng.2012.01.794.

[22] E.M. Wardhana, A. Santoso, A.R. Ramdani, Analysis of gottingen 428 airfoil turbine propeller design with computational fluid dynamics method on gravitational water vortex power plant, Int. J. Mar. Eng. Innov. Res. (2019), doi:10.12962/j25481479.v3i3.4864.

[23] T. Yavuz, E. Koç, B. Kilkiş, T. Erol, C. Balas, T. Aydemir, Performance analysis of the airfoil-slat arrangements for hydro and wind turbine applications, Renew. Energy 74 (2015) 414–421, doi:10.1016/j.renene.2014.08.049.

[24] K. Zhang, T. Wei, H. Hu, An experimental investigation on the surface water transport process over an airfoil by using a digital image projection technique, Exp. Fluids (2015), doi:10.1007/s00348-015-2046-z.

[25] W. Steinert, B. Eisenberg, H. Starken, Design and testing of a controlled diffusion airfoil cascade for industrial axial flow compressor application, J. Turbomach. (1991), doi:10.1115/1.2929119.

[26] H. Ma, C. Jin, L. Zhao, R. Ma, Effects of airfoil-probe tubes on the flow field of a compressor cascade, J. Therm. Sci. (2017), doi:10.1007/s11630-017-0945-4.

[27] K.H. Park, C.H. Park, Application of airfoil impeller for enhancement of aerodynamic performance of high speed centrifugal fan, Trans. Korean Soc. Mech. Eng. B (2016), doi:10.3795/KSME-B.2016.40.5.321.

[28] X. Xu, T. Ma, L. Li, M. Zeng, Y. Chen, Y. Huang, Q. Wang, Optimization of fin arrangement and channel configuration in an airfoil fin PCHE for supercritical CO2 cycle, Appl. Therm. Eng. 70 (2014) 867–875, doi:10.1016/j.applthermaleng.2014.05.040.

[29] F. Chen, L. Zhang, X. Huai, J. Li, H. Zhang, Z. Liu, Comprehensive performance comparison of airfoil fin PCHEs with NACA 00XX series airfoil, Nucl. Eng. Des. 315 (2017) 42–50, doi:10.1016/j.nucengdes.2017.02.014.

[30] X. Cui, J. Guo, X. Huai, K. Cheng, H. Zhang, M. Xiang, Numerical study on novel airfoil fins for printed circuit heat exchanger using supercritical CO2, Int. J. Heat Mass Transf. 121 (2018) 354–366, doi:10.1016/j.ijheatmasstransfer.2018.01.015.

[31] P. Selvakumar, S. Suresh, Convective performance of CuO/water nanofluid in an electronic heat sink, Exp. Therm Fluid Sci. 40 (2012) 57–63, doi:10.1016/j.expthermflusci.2012.01.033.

[32] C.J. Ho, W.C. Chen, An experimental study on thermal performance of Al2O3/water nanofluid in a minichannel heat sink, Appl. Therm. Eng. 50 (2013) 516–522, doi:10.1016/j.applthermaleng.2012.07.037.

[33] N.R. Kuppusamy, H.A. Mohammed, C.W. Lim, Numerical investigation of trapezoidal grooved microchannel heat sink using nanofluids, Thermochim. Acta 573 (2013) 39–56, doi:10.1016/j.tca.2013.09.011.

[34] B. Rimbault, C.T. Nguyen, N. Galanis, Experimental investigation of CuO-water nanofluid flow and heat transfer inside a microchannel heat sink, Int. J. Therm. Sci. 84 (2014) 275–292, doi:10.1016/j.ijthermalsci.2014.05.025.

[35] M.R. Sohel, S.S. Khaleduzzaman, R. Saidur, A. Hepbasli, M.F.M. Sabri, I.M. Mahbubul, An experimental investigation of heat transfer enhancement of a

minichannel heat sink using Al2O3–H2O nanofluid, Int. J. Heat Mass Transf. 74 (2014) 164–172, doi:10.1016/j.ijheatmasstransfer.2014.03.010.
[36] M.R. Sohel, R. Saidur, S.S. Khaleduzzaman, T.A. Ibrahim, Cooling performance investigation of electronics cooling system using Al2O3–H2O nanofluid, Int. Commun. Heat Mass Transf. 65 (2015) 89–93, doi:10.1016/j.icheatmasstransfer.2015.04.015.
[37] O. Mahian, E. Bellos, C.N. Markides, R.A. Taylor, A. Alagumalai, L. Yang, C. Qin, B.J. Lee, G. Ahmadi, M.R. Safaei, S. Wongwises, Recent advances in using nanofluids in renewable energy systems and the environmental implications of their uptake, Nano Energy 86 (2021) 106069, doi:10.1016/j.nanoen.2021.106069.
[38] S. Nabati Shoghl, J. Jamali, M. Keshavarz Moraveji, Electrical conductivity, viscosity, and density of different nanofluids: an experimental study, Exp. Therm Fluid Sci. 74 (2016) 339–346, doi:10.1016/j.expthermflusci.2016.01.004.
[39] H.M. Ali, M.D. Azhar, M. Saleem, Q.S. Saeed, A. Saieed, Heat transfer enhancement of car radiator using aqua based magnesium oxide nanofluids, Therm. Sci. 19 (2015) 2039–2048, doi:10.2298/TSCI150526130A.
[40] I.M. Mahbubul, E.B. Elcioglu, R. Saidur, M.A. Amalina, Optimization of ultrasonication period for better dispersion and stability of TiO2–water nanofluid, Ultrason. Sonochem. 37 (2017) 360–367, doi:10.1016/j.ultsonch.2017.01.024.
[41] A. Ghadimi, I.H. Metselaar, The influence of surfactant and ultrasonic processing on improvement of stability, thermal conductivity and viscosity of titania nanofluid, Exp. Therm Fluid Sci. 51 (2013) 1–9, doi:10.1016/j.expthermflusci.2013.06.001.
[42] N.I. Zouli, S.A.M. Mohammed, Enhancement of heat transfer coefficient using Fe2O3 – water, TechConnect Briefs 2 (2017) 247–250.
[43] N. Kumar, S.S. Sonawane, Experimental study of Fe2O3/water and Fe2O3/ethylene glycol nanofluid heat transfer enhancement in a shell and tube heat exchanger, Int. Commun. Heat Mass Transf. 78 (2016) 277–284, doi:10.1016/j.icheatmasstransfer.2016.09.009.
[44] T.X. Phuoc, M. Massoudi, Experimental observations of the effects of shear rates and particle concentration on the viscosity of Fe2O3-deionized water nanofluids, Int. J. Therm. Sci. 48 (2009) 1294–1301, doi:10.1016/j.ijthermalsci.2008.11.015.
[45] A. Parsian, M. Akbari, New experimental correlation for the thermal conductivity of ethylene glycol containing Al2O3–Cu hybrid nanoparticles, J. Therm. Anal. Calorim. 131 (2018) 1605–1613, doi:10.1007/s10973-017-6694-5.
[46] A. Asadi, M. Asadi, A. Rezaniakolaei, L.A. Rosendahl, M. Afrand, S. Wongwises, Heat transfer efficiency of Al2O3-MWCNT/thermal oil hybrid nanofluid as a cooling fluid in thermal and energy management applications: an experimental and theoretical investigation, Int. J. Heat Mass Transf. 117 (2018) 474–486, doi:10.1016/j.ijheatmasstransfer.2017.10.036.
[47] Y. Vermahmoudi, S.M. Peyghambarzadeh, S.H. Hashemabadi, M. Naraki, Experimental investigation on heat transfer performance of Fe2O3/water nanofluid in an air-finned heat exchanger, Eur. J. Mech. 44 (2014) 32–41, doi:10.1016/j.euromechflu.2013.10.002.
[48] W.H. Azmi, K.V. Sharma, P.K. Sarma, R. Mamat, S. Anuar, V. Dharma Rao, Experimental determination of turbulent forced convection heat transfer and friction factor with SiO2 nanofluid, Exp. Therm Fluid Sci. 51 (2013) 103–111, doi:10.1016/j.expthermflusci.2013.07.006.
[49] R.L. Hamilton, Thermal conductivity of heterogeneous two-component systems, Ind. Eng. Chem. Fundam. (1962), doi:10.1021/i160003a005.
[50] M. Corcione, Empirical correlating equations for predicting the effective thermal conductivity and dynamic viscosity of nanofluids, Energy Convers. Manage. (2011), doi:10.1016/j.enconman.2010.06.072.
[51] Y. Xuan, W. Roetzel, Conceptions for heat transfer correlation of nanofluids, Int. J. Heat Mass Transf. 43 (2000) 3701–3707, doi:10.1016/S0017-9310(99)00369-5.
[52] B.C. Pak, Y.I. Cho, Hydrodynamic and heat transfer study of dispersed fluids with submicron metallic oxide particles, Exp. Heat Transfer 11 (1998) 151–170, doi:10.1080/08916159808946559.
[53] G. Wang, J. Zhang, Thermal and power performance analysis for heat transfer applications of nanofluids in flows around cylinder, Appl. Therm. Eng. 112 (2017) 61–72, doi:10.1016/j.applthermaleng.2016.10.008.
[54] M. Corcione, M. Cianfrini, A. Quintino, Optimization of laminar pipe flow using nanoparticle liquid suspensions for cooling applications, Appl. Therm. Eng. 50 (2013) 857–867, doi:10.1016/j.applthermaleng.2012.07.029.
[55] W. Arshad, H.M. Ali, Experimental investigation of heat transfer and pressure drop in a straight minichannel heat sink using TiO2 nanofluid, Int. J. Heat Mass Transfer 110 (2017) 248–256, doi:10.1016/j.ijheatmasstransfer.2017.03.032.
[56] C. Cianfrini, M. Corcione, E. Habib, A. Quintino, Buoyancy-induced convection in Al2O3/water nanofluids from an enclosed heater, Eur. J. Mech. B. Fluids 48 (2014) 123–134, doi:10.1016/j.euromechflu.2014.04.014.
[57] A. Quintino, E. Ricci, E. Habib, M. Corcione, Buoyancy-driven convection of nanofluids in inclined enclosures, Chem. Eng. Res. Des. 122 (2017) 63–76, doi:10.1016/j.cherd.2017.04.007.
[58] W. Duangthongsuk, S. Wongwises, A dispersion model for predicting the heat transfer performance of TiO2–water nanofluids under a laminar flow regime, Int. J. Heat Mass Transfer 55 (2012) 3138–3146, doi:10.1016/j.ijheatmasstransfer.2012.02.016.
[59] P.K. Singh, P.V. Harikrishna, T. Sundararajan, S.K. Das, Experimental and numerical investigation into the hydrodynamics of nanofluids in microchannels, Exp. Therm Fluid Sci. 42 (2012) 174–186, doi:10.1016/j.expthermflusci.2012.05.004.
[60] R.S. Vajjha, D.K. Das, B.M. Mahagaonkar, Density measurement of different nanofluids and their comparison with theory, Pet. Sci. Technol. 27 (2009) 612–624, doi:10.1080/10916460701857714.
[61] S. Halelfadl, T. Maré, P. Estellé, Efficiency of carbon nanotubes water based nanofluids as coolants, Exp. Therm Fluid Sci. 53 (2014) 104–110, doi:10.1016/j.expthermflusci.2013.11.010.
[62] S. Suresh, K.P. Venkitaraj, P. Selvakumar, M. Chandrasekar, Synthesis of Al2O3-Cu/water hybrid nanofluids using two step method and its thermo physical properties, Colloids Surf. A 388 (2011) 41–48, doi:10.1016/j.colsurfa.2011.08.005.
[63] B. Takabi, S. Salehi, Augmentation of the heat transfer performance of a sinusoidal corrugated enclosure by employing hybrid nanofluid, Adv. Mech. Eng. 2014 (2014), doi:10.1155/2014/147059.
[64] M. Liu, D. Liu, S. Xu, Y. Chen, Experimental study on liquid flow and heat transfer in micro square pin fin heat sink, Int. J. Heat Mass Transf. 54 (2011) 5602–5611, doi:10.1016/j.ijheatmasstransfer.2011.07.013.
[65] R.S. Prasher, J. Dirner, J.-Y. Chang, A. Myers, D. Chau, D. He, S. Prstic, Nusselt number and friction factor of staggered arrays of low aspect ratio micropin-fins under cross flow for water as fluid, J. Heat Transf. 129 (2007) 141–153, doi:10.1115/1.2402179.
[66] A. Kosar, C.-J. Kuo, Y. Peles, Hydoroil-Based Micro Pin Fin Heat Sink, in: Proceedings of IMECE, 2008, pp. 563–570, doi:10.1115/imece2006-13257.
[67] A.Y. Gunter, W.A. Shaw, A general correlation of friction factors for various types of surfaces in cross flow, Trans. ASME. 67 (1945) 643–660.
[68] K.B. Anoop, T. Sundararajan, S.K. Das, Effect of particle size on the convective heat transfer in nanofluid in the developing region, Int. J. Heat Mass Transf. 52 (2009) 2189–2195, doi:10.1016/j.ijheatmasstransfer.2007.11.063.
[69] M.U. Sajid, H.M. Ali, A. Sufyan, D. Rashid, S.U. Zahid, W.U. Rehman, Experimental investigation of TiO2–water nanofluid flow and heat transfer inside wavy mini-channel heat sinks, J. Therm. Anal. Calorim. 137 (2019) 1279–1294, doi:10.1007/s10973-019-08043-9.
[70] W. Arshad, H.M. Ali, Graphene nanoplatelets nanofluids thermal and hydrodynamic performance on integral fin heat sink, Int. J. Heat Mass Transf. 107 (2017) 995–1001, doi:10.1016/j.ijheatmasstransfer.2016.10.127.
[71] K. Bashirnezhad, S. Bazri, M.R. Safaei, M. Goodarzi, M. Dahari, O. Mahian, A.S. Dalkılıça, S. Wongwises, Viscosity of nanofluids: a review of recent experimental studies, Int. Commun. Heat Mass Transf. 73 (2016) 114–123, doi:10.1016/j.icheatmasstransfer.2016.02.005.
[72] H. Babar, M. Sajid, H. Ali, Viscosity of hybrid nanofluids: a critical review, Therm. Sci. 23 (2019) 1713–1754, doi:10.2298/TSCI181128015B.
[73] M. Jarahnejad, E.B. Haghighi, M. Saleemi, N. Nikkam, R. Khodabandeh, B. Palm, M.S. Toprak, M. Muhammed, Experimental investigation on viscosity of water-based Al2O3 and TiO2 nanofluids, Rheol. Acta 54 (2015) 411–422, doi:10.1007/s00397-015-0838-y.
[74] C.T. Nguyen, F. Desgranges, G. Roy, N. Galanis, T. Maré, S. Boucher, H. Angue Mintsa, Temperature and particle-size dependent viscosity data for water-based nanofluids - Hysteresis phenomenon, Int. J. Heat Fluid Flow 28 (2007) 1492–1506, doi:10.1016/j.ijheatfluidflow.2007.02.004.
[75] Y. He, Y. Jin, H. Chen, Y. Ding, D. Cang, H. Lu, Heat transfer and flow behaviour of aqueous suspensions of TiO2 nanoparticles (nanofluids) flowing upward through a vertical pipe, Int. J. Heat Mass Transf. 50 (2007) 2272–2281, doi:10.1016/j.ijheatmasstransfer.2006.10.024.
[76] J. Zhao, Z. Luo, M. Ni, K. Cen, Dependence of nanofluid viscosity on particle size and pH value, Chin. Phys. Lett. 26 (2009) 066202.
[77] M. Hajj-Hassan, V.P. Chodavarapu, S. Musallam, Microfabrication of ultra-long reinforced silicon neural electrodes, Micro Nano Lett. 4 (2009) 53, doi:10.1049/mnl.
[78] A.A. Alfaryjat, H.A. Mohammed, N.M. Adam, D. Stanciu, A. Dobrovicescu, Numerical investigation of heat transfer enhancement using various nanofluids in hexagonal microchannel heat sink, Therm. Sci. Eng. Progress 5 (2018) 252–262, doi:10.1016/j.tsep.2017.12.003.
[79] Z. Azizi, A. Alamdari, M.R. Malayeri, Convective heat transfer of Cu-water nanofluid in a cylindrical microchannel heat sink, Energy Convers. Manage. 101 (2015) 515–524, doi:10.1016/j.enconman.2015.05.073.
[80] Q. Esmaili, A.A. Ranjbar, S. Porkhial, Experimental analysis of heat transfer in ribbed microchannel, Int. J. Therm. Sci. 130 (2018) 140–147, doi:10.1016/j.ijthermalsci.2018.04.020.
[81] S.M. Hassani, M. Khoshvaght-Aliabadi, S.H. Mazloumi, Influence of chevron fin interruption on thermo-fluidic transport characteristics of nanofluid-cooled electronic heat sink, Chem. Eng. Sci. 191 (2018) 436–447, doi:10.1016/j.ces.2018.07.010.
[82] M. Khoshvaght-Aliabadi, S.M. Hassani, S.H. Mazloumi, Comparison of hydrothermal performance between plate fins and plate-pin fins subject to nanofluid-cooled corrugated miniature heat sinks, Microelectron. Reliab. 70 (2017) 84–96, doi:10.1016/j.microrel.2017.01.005.
[83] N. Ahammed, L.G. Asirvatham, S. Wongwises, Thermoelectric cooling of electronic devices with nanofluid in a multiport minichannel heat exchanger, Exp. Therm Fluid Sci. 74 (2016) 81–90, doi:10.1016/j.expthermflusci.2015.11.023.
[84] H.M. Ali, W. Arshad, Thermal performance investigation of staggered and in-line pin fin heat sinks using water based rutile and anatase TiO 2 nanofluids, Energy Convers. Manage. 106 (2015) 793–803, doi:10.1016/j.enconman.2015.10.015.
[85] M. Khoshvaght-Aliabadi, S.M. Hassani, S.H. Mazloumi, M. Nekoei, Effects of nooks configuration on hydrothermal performance of zigzag channels for

nanofluid-cooled microelectronic heat sink, Microelectron. Reliab. 79 (2017) 153–165, doi:10.1016/j.microrel.2017.10.024.
[86] G. Xia, Y. Zhai, Z. Cui, Numerical investigation of thermal enhancement in a micro heat sink with fan-shaped reentrant cavities and internal ribs, Appl. Therm. Eng. 58 (2013) 52–60, doi:10.1016/j.applthermaleng.2013.04.005.
[87] L. Chai, G. Xia, M. Zhou, J. Li, J. Qi, Optimum thermal design of interrupted microchannel heat sink with rectangular ribs in the transverse microchambers, Appl. Therm. Eng. 51 (2013) 880–889, doi:10.1016/j.applthermaleng.2012.10.037.
[88] T. Ambreen, M.-H. Kim, Effect of fin shape on the thermal performance of nanofluid-cooled micro pin-fin heat sinks, Int. J. Heat Mass Transf. 126 (2018) 245–256, doi:10.1016/j.ijheatmasstransfer.2018.05.164.
[89] Y. Sui, P.S. Lee, C.J. Teo, An experimental study of flow friction and heat transfer in wavy microchannels with rectangular cross section, Int. J. Therm. Sci. 50 (2011) 2473–2482, doi:10.1016/j.ijthermalsci.2011.06.017.
[90] H. Ermagan, R. Rafee, Geometric optimization of an enhanced microchannel heat sink with superhydrophobic walls, Appl. Therm. Eng. 130 (2018) 384–394, doi:10.1016/j.applthermaleng.2017.11.039.
[91] H. Ermagan, R. Rafee, Effect of pumping power on the thermal design of converging microchannels with superhydrophobic walls, Int. J. Therm. Sci. 132 (2018) 104–116, doi:10.1016/j.ijthermalsci.2018.05.051.